Plant Cell Advance Publication. Published on March 4, 2020, doi:10.1105/tpc.19.00992

RESEARCH ARTICLE

Mutagenesis of a Quintuple Mutant Impaired in Environmental Responses Reveals Roles for *CHROMATIN REMODELING4* in the Arabidopsis Floral Transition

Qing Sang[a,*], Alice Pajoro[a,*], Hequan Sun[a], Baoxing Song[a], Xia Yang[a,b], Sara C Stolze[a], Fernando Andrés[a,c], Korbinian Schneeberger[a], Hirofumi Nakagami[a] and George Coupland[a,#]

[a]Max Planck Institute for Plant Breeding Research, Carl-von-Linné-Weg 10, D50829, Germany
[b] State Key Laboratory of Systematic and Evolutionary Botany, Institute of Botany, Chinese Academy of Sciences, Xiangshan, Beijing 100093, China
[c] AGAP, Univ. Montpellier, CIRAD, INRA, Montpellier SupAgro, Montpellier, France
*These authors contributed equally to this work.
[#]Corresponding author. E-mail: coupland@mpipz.mpg.de

Short Title: Role of *CHR4* in the floral transition

One Sentence Summary: A genetic screen employed to identify genes that regulate flowering independently of environmental cues revealed a role for the chromatin remodeler CHR4 in promoting floral identity.

The author responsible for distribution of materials integral to the findings presented in this article in accordance with the policy described in the Instructions for Authors (www.plantcell.org) is George Coupland (coupland@mpipz.mpg.de)

ABSTRACT

Several pathways conferring environmental flowering responses in *Arabidopsis thaliana* converge on developmental processes that mediate the floral transition in the shoot apical meristem. Many characterized mutations disrupt these environmental responses, but downstream developmental processes have been more refractory to mutagenesis. Here, we constructed a quintuple mutant impaired in several environmental pathways and showed that it possesses severely reduced flowering responses to changes in photoperiod and ambient temperature. RNA-seq analysis of the quintuple mutant showed that the expression of genes encoding gibberellin biosynthesis enzymes and transcription factors involved in the age pathway correlates with flowering. Mutagenesis of the quintuple mutant generated two late-flowering mutants, *quintuple ems 1* (*qem1*) and *qem2*. The mutated genes were identified by isogenic mapping and transgenic complementation. The *qem1* mutant is an allele of the gibberellin 20-oxidase gene *ga20ox2*, confirming the importance of gibberellin for flowering in the absence of environmental responses. By contrast, *qem2* is impaired in *CHROMATIN REMODELING4* (*CHR4*), which has not been genetically implicated in floral induction. Using co-immunoprecipitation, RNA-seq and ChIP-seq, we show that CHR4 interacts with transcription factors involved in floral meristem identity and affects the expression of key floral regulators. Therefore,

CHR4 mediates the response to endogenous flowering pathways in the inflorescence meristem to promote floral identity.

INTRODUCTION

Lateral shoot organs initiate from cells on the flanks of the shoot apical meristem (SAM), and the identity of the formed organs changes during development (Bowman and Eshed, 2000). In *Arabidopsis thaliana*, the transition from vegetative leaf initiation to flower production occurs in response to several environmental and endogenous cues. Important environmental signals that control flowering include seasonal fluctuations in temperature and day length, which are mediated by the photoperiodic and vernalization pathways, whereas ambient changes in temperature also influence flowering time (Srikanth and Schmid, 2011; Andres and Coupland, 2012). In addition, endogenous signals such as gibberellins (GAs) and the age of the plant contribute to the floral transition in the absence of inductive environmental cues (Wilson et al., 1992; Wang et al., 2009).

Three intersecting environmental pathways that promote flowering have been well characterized. The photoperiodic pathway promotes flowering under long days (LDs) but not under short days (SDs), in which plants flower much later. Exposure to LDs stabilizes the CONSTANS transcription factor (Valverde et al., 2004), which in turn activates transcription of *FLOWERING LOCUS T* (*FT*) and *TWIN SISTER OF FT* (*TSF*) in the leaf vascular tissue (Kardailsky et al., 1999; Kobayashi et al., 1999; Suarez-Lopez et al., 2001; An et al., 2004; Yamaguchi et al., 2005). The FT and TSF proteins, which are related to phophatidyl-ethanolamine binding proteins, move to the SAM (Corbesier et al., 2007; Jaeger and Wigge, 2007; Mathieu et al., 2007), where they physically interact with the bZIP transcription factor FD (Abe et al., 2005; Wigge et al., 2005; Abe et al., 2019). In the SAM, the FT–FD protein complex promotes the transcription of genes encoding floral activators, such as *SUPPRESSOR OF OVEREXPRESSION OF CO1* (*SOC1*) and *FRUITFULL* (*FUL*), which induce the floral transition, as well as *APETALA1* (*AP1*) and *LEAFY* (*LFY*), which promote floral meristem identity (Schmid et al., 2003; Wigge et al., 2005; Torti et al., 2012; Collani et al., 2019). Because they represent the mobile signal linking leaves and the shoot apical meristem, FT and TSF are essential for the photoperiodic flowering response, and *ft tsf* double mutants are daylength-insensitive (Yamaguchi et al., 2005; Jang et al., 2009).

The seasonal cue of exposure to winter cold mediates flowering via the vernalization pathway, which represses transcription of the floral repressor *FLOWERING LOCUS C* (*FLC*) (Michaels and Amasino, 1999; Sheldon et al., 1999). FLC is a MADS-box transcription factor that forms regulatory complexes with other MADS-box floral repressors, such as SHORT VEGETATIVE PHASE (SVP) (Li et al., 2008). Thus, vernalization reduces *FLC* transcription and promotes flowering via the endogenous and photoperiodic pathways, whereas mutants for *FLC* are essentially insensitive to vernalization. The genome-wide binding sites of FLC and SVP include those in several genes that promote flowering within the photoperiodic pathway, such as *FT* and *SOC1* (Searle et al., 2006; Lee et al., 2007; Li et al., 2008; Deng et al., 2011; Mateos et al., 2015; Richter et al., 2019). Because *FLC* is stably repressed by exposure to cold, plants can flower through the photoperiodic pathway when they are exposed to LDs after cold exposure. Also, genes within the endogenous pathway that are repressed by FLC, such as *SQUAMOSA PROMOTER BINDING PROTEIN-LIKE15* (*SPL15*), can promote flowering during vernalization (Deng et al., 2011; Hyun et al., 2019)

Arabidopsis also flowers rapidly when exposed to high temperatures, and this response can overcome the delay in flowering observed under SDs at lower growth temperatures (Balasubramanian et al., 2006). *FT* and *TSF* are transcribed at high temperature under SDs and promote early flowering; thus their transcriptional repression under SDs at lower temperatures is overcome at high temperatures (Kumar et al., 2012; Galvao et al., 2015; Fernandez et al., 2016). Accordingly, MADS-box repressors of *FT* and *TSF*, particularly FLOWERING LOCUS M and SVP, do not accumulate under SDs at high temperature, and mutations in these genes reduce the flowering response to high temperature (Lee et al., 2007; Lee et al., 2013; Pose et al., 2013; Airoldi et al., 2015). The reduced activity of these repressors also enhances the response of the meristem to low levels of *FT* and *TSF* transcription in the leaves (Fernandez et al., 2016). Triple mutants for *FT, TSF* and *SVP* are insensitive to higher temperatures under SDs (Fernandez et al., 2016).

In addition to these environmental pathways, there are several endogenous flowering pathways. A set of genes was ascribed to the autonomous flowering pathway, because they caused late-flowering under LDs and SDs and were therefore considered to promote flowering independently of photoperiodic cues (Koornneef et al., 1991). Mutations in all these genes caused elevated levels of *FLC* mRNA, and

66 the encoded proteins contribute to *FLC* expression at the transcriptional and post-
67 transcriptional levels (Whittaker and Dean, 2017). The late-flowering phenotype of
68 autonomous pathway mutants can therefore be suppressed by mutations in *FLC*
69 (Michaels and Amasino, 2001). In addition, gibberellin (GA) is an important
70 contributor to endogenous flowering regulation, because mutations or transgenes
71 that strongly reduce GA levels almost abolished flowering under non-inductive SDs
72 (Wilson et al., 1992; Galvao et al., 2012; Porri et al., 2012). Finally, microRNA156
73 (miR156) negatively regulates the floral transition and is developmentally regulated
74 such that its abundance decreases progressively with increasing plant age (Wu and
75 Poethig, 2006; Wang et al., 2009). This miRNA negatively regulates the
76 accumulation of several SPL transcription factors, including SPL3, SPL9 and SPL15,
77 which promote the floral transition, particularly under non-inductive SDs (Gandikota
78 et al., 2007; Wang et al., 2009; Yamaguchi et al., 2009; Hyun et al., 2016; Xu et al.,
79 2016). Thus, miR156/SPL modules have been associated with an endogenous
80 flowering pathway related to plant age.

81 Here, we extend our understanding of the genetic basis of the floral transition
82 by screening specifically for genes that regulate flowering independently of the
83 environmental pathways. To this end, we constructed a high-order quintuple mutant,
84 *svp-41 flc-3 ft-10 tsf-1 soc1-2*, which shows reduced sensitivity to environmental
85 flowering signals because it is impaired in responses to photoperiod and high
86 temperature. Using RNA-seq, we characterized the expression of flowering-related
87 genes in this mutant, and we employed a forward genetics approach to identify
88 genes controlling flowering time in this background. This allowed us to define a role
89 for CHROMATIN REMODELING4 (CHR4) in promoting the floral transition.

90 RESULTS

91 Phenotypic and molecular characterization of a quintuple mutant strongly 92 impaired in responses to environmental cues

93 To assess the flowering time of Arabidopsis plants in which the major environmental
94 pathways were inactivated, we constructed the quintuple mutant *svp-41 flc-3 ft-10 tsf-*
95 *1 soc1-2* (hereafter referred to as the quintuple mutant). The quintuple mutant
96 showed a dramatically reduced flowering response to day length compared to Col-0.
97 Under long days (LDs), the quintuple mutant bolted later and after forming more
98 vegetative rosette leaves than the wild type (Col-0) (**Figure 1A and B**). However,

99 under short days (SDs) at 21°C, the mutant bolted much earlier than Col-0 in terms
100 of days to flowering and rosette leaf number (**Figure 1A and B**). Bolting of the
101 quintuple mutant was delayed by fewer than 10 days in SDs compared to LDs,
102 whereas bolting in Col-0 was delayed by approximately 50 days. Similarly, the
103 quintuple mutant formed ~5 more rosette leaves under SDs than LDs, whereas Col-0
104 formed over 40 more rosette leaves. The flowering time of the quintuple mutant was
105 also insensitive to higher ambient temperatures under SDs when considering bolting
106 time, but it displayed partial insensitivity in terms of rosette leaf number (**Figure 1A**
107 **and B**). Finally, GA_4 treatment accelerated flowering of Col-0 under SDs (Wilson et
108 al., 1992) but had a smaller effect on the flowering time of the quintuple mutant
109 (**Supplemental Figure 1A and B**). These results are consistent with the idea that the
110 GA response and signaling are activated in the quintuple mutant, as previously
111 shown for *svp-41* mutants (Andres et al., 2014). Overall, the quintuple mutant
112 showed strongly impaired responses to environmental signals such as day-length
113 and ambient temperatures, in terms of time to bolting and the number of rosette
114 leaves formed. These data suggest that in the quintuple mutant, the floral transition
115 occurs via endogenous mechanisms such as the GA or age pathway.

116 In addition to effects on bolting time and vegetative rosette leaf number, the
117 quintuple mutant produced more cauline leaves than Col-0 in all conditions tested
118 (**Supplemental Figure 1C**). The quintuple mutant formed on average 4.5-fold more
119 cauline leaves than Col-0 under LDs and 2.3-fold more under SDs. The increased
120 cauline leaf number in the mutant compared with Col-0 suggests that the mutant is
121 also impaired in the determination of floral meristem identity after floral induction and
122 bolting, such that more phytomers contain cauline leaves and axillary shoots than in
123 Col-0.

124 We then compared the developmental stage of the shoot apex of the quintuple
125 mutant to that of Col-0 by performing *in situ* hybridizations for *FUL* transcript on
126 apical cross-sections of SD-grown plants of different ages (**Figure 1C**). *FUL* encodes
127 a MADS-box floral activator that is partially genetically redundant with *SOC1*. *FUL*
128 mRNA accumulates in the SAM during the early stages of the floral transition
129 (Ferrandiz et al., 2000; Melzer et al., 2008; Torti et al., 2012). In the apices of SD-
130 grown plants, *FUL* mRNA accumulated approximately one-week earlier in the
131 quintuple mutant than in Col-0 (**Figure 1C**), which is consistent with the earlier
132 flowering phenotype of the mutant.

133 Because the quintuple mutant flowers earlier under SDs and major regulators
134 of flowering are inactivated, the transcriptional network associated with the floral
135 transition is probably differentially expressed in the mutant compared to Col-0. To
136 define these differences, we performed RNA-seq on apices of the quintuple mutant
137 and Col-0 through a developmental time course under SDs. Apical samples were
138 harvested from both genotypes 3, 4, 5 and 6 weeks after sowing. In vegetative
139 apices of both genotypes at 3 weeks after sowing, only 46 genes were differentially
140 expressed (adjp-value < 0.05) (DEGs) between the quintuple mutant and Col-0. At 4,
141 5 and 6 weeks, when the mutant flowered more rapidly than Col-0 (**Figure 1C**), 486,
142 736 and 568 genes, respectively, were differentially expressed in the mutant
143 compared with Col-0 (**Supplemental Data Set 1**). At these time points,
144 approximately 45%, 14% and 33% of the DEGs, respectively, were more highly
145 expressed in the quintuple mutant vs. Col-0 (**Supplemental Data Set 1**). The
146 mRNAs of *SPL3, SPL4, SPL5, SPL9, SPL12* and *SPL15*, which are regulated by
147 miR156 and contribute to the endogenous age-related flowering pathway, were more
148 abundant in the quintuple mutant, which is consistent with promotion of flowering by
149 the age pathway (**Figure 1D and E**). Moreover, the floral activators *FD*, *FDP* and
150 *AGAMOUS-LIKE6* (*AGL6*) were more highly expressed in the mutant vs. Col-0
151 (**Figure 1D and E, Supplemental Figure 1D and Supplemental Data Set 1**), and
152 the expression of the floral repressors *MADS-AFFECTING FLOWERING 4* (*MAF4*)
153 and *MAF5* was attenuated in the quintuple mutant (**Supplemental Data Set 1**).
154 Moreover, genes encoding enzymes involved in GA biosynthesis and catabolism
155 were differentially expressed in the quintuple mutant (**Figure 1D**).

156 **A sensitized mutant screen in the quintuple mutant background identifies two**
157 **loci that promote flowering**

158 We then employed the quintuple mutant as a sensitized background for mutagenesis
159 screening to identify genes that regulate flowering independently of environmental
160 pathways. This approach was expected to identify mutations in endogenous
161 components, because the major environmental floral response pathways are already
162 impaired in the mutant, and mutations in the autonomous pathway should not be
163 recovered, because *FLC* is inactive in the quintuple mutant. We screened the M_2
164 generation for mutants with altered flowering behaviour (Methods). Two mutants
165 showing delayed floral transition in the quintuple mutant background, *quintuple ems 1*

166 (*qem1*) and *quintuple ems 2* (*qem2*), were selected for detailed studies because they
167 exhibited strong and reproducible phenotypes in the M_3 generation. Both lines
168 segregated the mutant phenotype in a 3:1 ratio in the $BC1F_2$ generation (Methods),
169 suggesting that a single recessive mutation was responsible for the phenotypes of
170 both mutants. Plants segregating the *qem1* or *qem2* phenotype in the respective
171 $BC1F_2$ populations were then bulk-harvested. Fast-isogenic mapping (Methods)
172 (Hartwig et al., 2012) localized *qem1* and *qem2* with high confidence to different
173 regions on chromosome 5 (**Supplemental Figure 2 and Figure 2**).

174 The *qem1* mutation localized to the same region of chromosome 5 as the
175 gibberellin 20-oxidase gene *GA20ox2* (**Supplemental Figure 2C and Supplemental**
176 **Table 1**). Mutation of *GA20ox2* delays flowering and has a stronger effect in the *svp-*
177 *41* background (Rieu et al., 2008; Plackett et al., 2012; Andres et al., 2014). In *qem1*,
178 a single nucleotide polymorphism was identified in the first exon of *GA20ox2* that was
179 predicted to cause an amino-acid substitution in the protein (ser137asn). To confirm
180 that this mutation causes the late-flowering phenotype of *qem1*, we performed
181 molecular complementation. Introducing the Col-0 genomic *GA20ox2* locus into
182 *qem1* strongly reduced leaf number and flowering time, so that the transgenic lines
183 flowered at a similar time or earlier than the quintuple mutant (**Supplemental Figure**
184 **2D and E**), confirming that the mutation in GA20ox2 was responsible for the delayed
185 flowering of *qem1*. This result is consistent with the RNA-seq data showing that
186 *GA20ox2* mRNA is more highly expressed in the quintuple mutant background than
187 in Col-0 (**Supplemental Figure 1D** and with the previous observation that *svp-41*
188 mutants contain higher levels of bioactive GAs than the wild type (Andres et al.,
189 2014). Therefore, the GA pathway likely plays a decisive role in promoting the floral
190 transition in the quintuple mutant.

191 The *qem2* mutant was later flowering and initiated more rosette and cauline
192 leaves than the quintuple mutant (**Figure 2A and B**), indicating a delay in the floral
193 transition and impaired floral meristem identity. The region of chromosome 5 to which
194 *qem2* mapped contained no previously described flowering-time genes (**Figure 2C**
195 **and Table 1**). Three high-confidence polymorphisms predicted to cause non-
196 synonymous mutations in the coding sequences *At5g43450*, *At5g44690* and
197 *At5g44800* were identified (**Table 1**). *At5g43450* encodes a protein with similarity to
198 ACC oxidase, *At5g44690* encodes a protein of unknown function, and *At5g44800*
199 encodes the CHD3-like ATP-dependent chromatin-remodelling factor CHR4. In

200 Arabidopsis, CHR4 is most closely related to PICKLE (PKL), which represses
201 flowering via the GA pathway (Fu et al., 2016; Park et al., 2017) and promotes
202 flowering via the photoperiodic pathway though *FT* activation (Jing et al., 2019a; Jing
203 et al., 2019b). Both PKL and CHR4 are homologous to SWI/SWF nuclear-localized
204 chromatin remodelling factors of the CHD3 family (Ogas et al., 1999), and *CHR4* is
205 also named *PICKLE RELATED1* (*PKR1*) (Aichinger et al., 2009). The *chr4* mutant
206 shows no obvious mutant phenotype under standard growth conditions (Aichinger et
207 al., 2009). However, CHR4 function has been implicated in floral organ development
208 because it interacts with the MADS-domain transcription factors AGAMOUS (AG),
209 APETALA3 (AP3), PISTILLATA (PI), SEPALLATA3 (SEP3), and AP1, as revealed by
210 immunoprecipitation of these factors (Smaczniak et al., 2012). Therefore, we
211 hypothesized that the mutation in *CHR4* caused the *qem2* mutant phenotype. We
212 tested this by introducing *pCHR4:CHR4* and *pCHR4:CHR4-VENUS* constructs into
213 *qem2*. The increased leaf number phenotype of *qem2* was reduced to a similar
214 number as in the progenitor quintuple mutant in all transformed lines (**Figure 2D**).
215 Thus, we conclude that the later-flowering *qem2* phenotype was caused by the
216 mutation in *CHR4*.

217 **Phenotypic characterization of *chr4* and its effects on gene expression during**
218 **floral induction**

219 The *qem2* mutant contains a mutation in the SNF2-related helicase/ATPase domain
220 of CHR4, resulting in the substitution of a conserved alanine (ala) residue by valine
221 (val) (ala713val) (**Figure 3A**). To analyze the *chr4* mutant phenotype in the Col-0
222 background, we characterized the T-DNA insertion allele *chr4-2* (SAIL_783_C05),
223 containing a T-DNA insertion within the coding sequence between the
224 helicase/ATPase domain and the DNA-binding domain (**Figure 3A**). The T-DNA
225 insertion also causes a reduction in *CHR4* mRNA levels (**Supplemental Figure 3**).

226 We compared the leaf number, bolting time, and flowering time of *qem2* and
227 *chr4-2* with those of their respective progenitors under LDs (**Supplemental Figure**
228 **4A, B**) and SDs (**Figures 3B–E**). The *qem2* mutant formed approximately 20 more
229 rosette leaves and 30 more cauline leaves than the quintuple mutant under both LDs
230 and SDs (**Figure 3B, C and Supplemental Figure 4A, B**). Despite having more
231 rosette leaves, the bolting time of *qem2* was similar to that of its progenitor (**Figure**
232 **3D**), whereas time to first open flower was markedly delayed in *qem2* (**Figure 3D, F**),

233 which is consistent with the increased number of cauline leaves. The phenotypic
234 difference between Col-0 and *chr4-2* was less severe than that between *qem2* and
235 the quintuple mutant. Under LDs, *chr4-2* and Col-0 initiated a similar number of
236 leaves (**Supplemental Figure 4B**). Under SDs, *chr4-2* and Col-0 had a similar
237 rosette leaf number, but *chr4-2* bolted earlier and produced more cauline leaves
238 **(Figure 3B–E**). CHR4 function appeared to be more important for flowering control in
239 the quintuple mutant background, suggesting it might preferentially regulate flowering
240 via the GA and aging pathways.

241 The *chr4-2* and *qem2* mutants bolted slightly earlier than their progenitors but
242 initiated a similar number or more rosette leaves (**Figure 3B and D**), suggesting that
243 they might have a shorter plastochron and initiate rosette leaves more rapidly. To
244 determine the plastochron, we counted rosette leaves weekly until the plants bolted
245 under SDs. Early in rosette development, *chr4-2* and *qem2* produced leaves at a
246 similar rate as their progenitors, but later in rosette development, the mutants
247 produced leaves more rapidly than the progenitors, leading to a steep increase in leaf
248 number (**Figure 3G and H**). More rapid leaf initiation can be related to an enlarged
249 SAM (Barton, 2010); therefore, we compared the SAMs of *chr4*-2 and *qem2* to those
250 of Col-0 and the quintuple mutant, respectively, after 4 and 5 weeks of growth under
251 SDs (**Supplemental Figure 5**). The SAMs of plants carrying either *chr4* mutant allele
252 were larger than those of their progenitors, but this was most pronounced for *qem2*
253 compared with the quintuple mutant (**Supplemental Figure 5**).

254 The transition to flowering in Arabidopsis can be conceptualised as two
255 sequential steps in which the inflorescence meristem acquires different identities.
256 After the transition from a vegetative meristem, the inflorescence meristem (I_1)
257 initially forms cauline leaves and axillary branches, and after transition from I_1 to I_2, it
258 initiates floral primordia (Ratcliffe et al., 1999). Rosette leaf number and days to
259 bolting can be used as a proxy for the I_1 transition, whereas the number of cauline
260 leaves produced on the flowering stem and days to the first open flower indicate
261 when the I_1 to I_2 transition occurs. Cauline leaves can be distinguished from rosette
262 leaves due to their smaller size and more pointed shape, so that the increased
263 number of leaves on the inflorescence stem can be explained by a delayed I_2
264 transition rather than by enhanced internode elongation between rosette leaves.
265 Compared to Col-0, *chr4-2* is not delayed in the transition from vegetative meristem
266 to I_1 but is delayed in the transition from I_1 to I_2. By contrast, compared to the

267 quintuple mutant, *qem2* mutants were strongly delayed in both the transition to I_1 and
268 to I_2 (**Figure 3B–E**).

269 In Arabidopsis, *AP1* confers floral meristem identity and is a marker for the I_1
270 to I_2 transition; therefore, we performed *in situ* hybridizations to monitor the
271 appearance of *AP1* mRNA through a developmental time course (**Figure 4**). At 5
272 weeks after germination, no *AP1* expression was detected in any of the genotypes,
273 indicating that the plant meristems were still vegetative. *AP1* mRNA was detected at
274 6 weeks in Col-0 and *chr4-2*. In *qem2* mutants, *AP1* mRNA appeared more than 1
275 week later than in the quintuple mutant, which is consistent with observation that
276 more cauline leaves formed in *qem2* (**Figure 4**).

277 We then performed RNA-seq along a developmental time course to identify
278 the genome-wide effects of CHR4 on gene expression during the floral transition. We
279 examined the transcriptomes of shoot apices of Col-0, the quintuple mutant*, chr4-2,*
280 and *qem2* plants grown for 3, 4, 5, or 6 weeks under SDs and compared the *chr4-2*
281 and *qem2* transcriptomes to those of Col-0 and the quintuple mutant, respectively
282 (**Supplemental Data Set 2**). The analysis focused on 237 genes previously reported
283 to regulate the floral transition in Arabidopsis (Bouche et al., 2016). In total, 26 of
284 these genes were significantly differentially (adjp-value < 0.05 and log2FC |1|)
285 expressed genes (DEGs) between *chr4-2* and Col-0 (**Figure 5A**), and 18 were DEGs
286 between *qem2* and the quintuple mutant (**Figure 5C**). Nine genes were common to
287 the two lists (*AGL79*, *BRANCHED1* (*BRC1*), *FUL*, *SEP3*, *AGL17*, *SPL4*, *BROTHER*
288 *OF FT AND TFL1* (*BFT*), *EARLY FLOWERING 4* (*ELF4*) and *MAF4*). The expression
289 of *SPL4*, which encodes a component of the age-dependent flowering pathway,
290 increased at several time points in the *chr4* and *qem2* mutants compared to their
291 respective progenitors (**Figure 5A–D**). In particular, *SPL4* was most highly expressed
292 in 4-week-old *qem2* and in 5-week-old *chr4*-2 plants (**Figure 5B–D**). *FUL* was also
293 more highly expressed in both mutants at later time points (**Figure 5B and D**) and is
294 a direct target of SPL9, SPL15, and SPL3 during the floral transition (Wang et al.,
295 2009; Yamaguchi et al., 2009; Hyun et al., 2016). Indeed, a corresponding small
296 increase in mRNA levels of *SPL9* and *SPL15* was also observed in the *CHR4*
297 mutants (**Supplemental Data Set 2**). The earlier increase in expression of *SPL4*,
298 *SPL9*, and *SPL15* is consistent with the earlier bolting observed in the mutants, as
299 *qem2* bolted around two days and *chr4*-2 around 10 days earlier than their respective
300 progenitors (**Figure 3D**).

301 We detected elevated expression of *TERMINAL FLOWER1* (*TFL1*) in *chr4*-2
302 (**Figure 5A and B**) and *BFT* in *qem2* (**Figure 5C**). Overexpression of *TFL1* and *BFT*,
303 which both encode proteins related to phosphatidylethanolamine-binding proteins,
304 reduces *AP1* and *LFY* expression and delays floral organ initiation (Ratcliffe et al.,
305 1998; Yoo et al., 2010). Consistent with this finding, *LFY* mRNA was also less
306 abundant in *qem2* (**Figure 5D**). During the inflorescence meristem transition from I_1
307 to I_2, increased LFY activity induces floral meristem identity by directly activating *AP1*
308 transcription and reducing GA levels, such that SPL9 recruits DELLA proteins to the
309 regulatory region of *AP1* (Weigel et al., 1992; Wagner et al., 1999; Yamaguchi et al.,
310 2014). Therefore, in the absence of CHR4 function, attenuated *LFY* transcription
311 likely contributes to a delay in the transition to the I_2 phase, as reflected by the
312 increased number of cauline leaves in *qem2*.

313 **CHR4 protein localisation *in planta* and identification of *in vivo* protein**
314 **interactors of CHR4**

315 Chromatin remodelers are often recruited to target genes by specific transcription
316 factors. Therefore, to further understand its mode of action during the floral transition,
317 we identified proteins that interact with CHR4. We used the transgenic plants
318 described above that express a fusion of VENUS fluorescent protein and CHR4
319 expressed from its native promoter (*pCHR4:CHR4-VENUS*). We analyzed the
320 expression pattern of this CHR4-VENUS protein by confocal microscopy and
321 compared it to the results of *in situ* hybridization analysis of *CHR4* mRNA. CHR4-
322 VENUS was localized to the nucleus and its spatial pattern was similar to the mRNA
323 pattern detected by *in situ* hybridization in the SAM, floral organs, and young leaves
324 (**Supplemental Figure 6**).

325 To identify protein interactors, we immunoprecipitated CHR4-VENUS protein
326 from inflorescence tissue and 5-week-old SD apical-enriched tissue using anti-GFP
327 antibodies and used p35S-YFP transgenic plants as a negative control. Proteins that
328 specifically co-immunoprecipitated with CHR4-VENUS were identified by protein
329 mass spectrometry (Methods). In total, 136 and 342 proteins were significantly (FDR
330 = 0.01) enriched in inflorescences and 5-week-old SD apex enriched tissue,
331 respectively. The CHR4-interacting proteins in inflorescences included the floral
332 homeotic MADS-domain transcription factors AP1, SEP3, PI and AP3 (**Table 2 and**
333 **Supplemental Data Set 3**). The reciprocal experiment of immunoprecipitating AP1

334 was performed with g*AP1:GFP* plants and CHR4 was detected among the
335 coimmunoprecipitated proteins (**Supplemental Data Set 3 and Supplemental**
336 **Figure 7**). Taken together, these results confirm the previous finding that CHR4
337 could be co-immunoprecipitated with AG, AP3, PI, SEP3 and AP1 (Smaczniak et al.,
338 2012). Moreover, SEP1 and SEP2 were also found here to be interaction partners of
339 CHR4 in inflorescence tissues (**Table 2, Supplemental Data Set 3, Supplemental**
340 **Figure 7**). In addition to floral homeotic proteins, other MADS-domain proteins were
341 found to interact with CHR4 in inflorescences, including AGL6 and the fruit- and
342 ovule-specific protein SHATTERPROOF2 (SHP2) (Favaro et al., 2003) (**Table 2,**
343 **Supplemental Data Set 3, Supplemental Figure 7**).
344 Other classes of transcription factors involved in the floral transition were
345 identified in CHR4 complexes. Notably, SPL2, SPL8, and SPL11 were found to be
346 interaction partners in inflorescences, whereas SPL13 was identified as a partner in
347 inflorescences and enriched apices (**Table 2, Supplemental Data Set 3,**
348 **Supplemental Figure 7**). Furthermore, TARGET OF EARLY ACTIVATION
349 TAGGED1 (TOE1), an AP2-domain transcription factor that represses the floral
350 transition (Aukerman and Sakai, 2003), also interacted with CHR4 in enriched apices.
351 A further list of transcription factors and chromatin remodellers identified as CHR4
352 interactors is provided in Table 2 and Supplemental Data Set 3.
353 These experiments demonstrated that CHR4 associates *in vivo* with several
354 transcription factors of the MADS, SPL, and AP2 classes that contribute to the floral
355 transition and floral meristem identity.

356 **Genome-wide effects of CHR4 on histone modifications and gene expression**

357 Proteins from the CHD3 group that includes CHR4 can participate in different
358 chromatin remodelling pathways and either repress or activate gene expression,
359 depending on the factors with which they associate. For example, PKL associates
360 with genes enriched in trimethylation of histone H3 lysine 27 (H3K27me3), which is
361 related to gene repression (Zhang et al., 2008; Zhang et al., 2012), and maintains
362 this epigenetic state (Carter et al., 2018). In addition, PKL reduces H3K27me3 at
363 specific target genes in particular tissues and environments (Jing et al., 2013).
364 Changes in H3K27me3 and H3K4me3 were also reported in the rice (*Oryza sativa*)
365 mutant of a CHR4 homologue (Hu et al., 2012). To test whether CHR4 regulates
366 gene expression by influencing histone modifications, we compared global

367 H3K27me3 and H3K4me3 levels in Col-0 and *chr4*-2 plants (**Supplemental Figure**
368 **8**). No clear difference in the global frequency of these histone marks was observed
369 between the two genotypes, suggesting that CHR4 does not affect the total
370 accumulation of these histone modifications.

371 To test whether CHR4 affects the deposition of these histone marks at specific
372 loci, we performed chromatin immunoprecipitation sequencing (ChIP-seq) to
373 compare genome-wide H3K27me3 and H3K4me3 levels in Col-0 and *chr4-2*.
374 H3K27me3 and H3K4me3 ChIP-seq experiments were performed on three biological
375 replicates for each genotype (see Methods). In total, 10,194 H3K27me3-marked
376 regions and 15,992 H3K4me3-marked regions were identified in the two genotypes
377 (**Supplemental Data Set 4**). Quantitative comparison with DANPOS2 (Chen et al.,
378 2013) revealed a subset of regions with significant differences (FDR < 0.05) in
379 H3K27me3 or H3K4me3 levels between Col-0 and *chr4*-2. In total, 857 regions were
380 differentially marked with H3K27me3 and 1,032 regions were differentially marked
381 with H3K4me3 (**Supplemental Data Set 4**). Notably, hypermethylated as well as
382 hypomethylated regions were identified in *chr4*-2 (**Figure 6A**). The genes
383 differentially marked with H3K27me3 included regulators of key hormonal pathways
384 involved in the floral transition, such as *GIBBERELLIN 3-OXIDASE1* (*GA3ox1*) and
385 *GA3ox4*, which encode GA biosynthesis enzymes. Genes encoding components of
386 auxin signalling (*ETTIN* (*ETT*) and *AUXIN RESISTANT 1* (*AUX1*)) and an enzyme
387 that catabolises cytokinin (*CYTOKININ OXIDASE 5* (*CKX5*)) were also differentially
388 marked with H3K27me3 in *chr4*-2 (**Supplemental Data Set 4**). Genes differentially
389 marked with H3K4me3 included the regulators of the floral transition *SPL15*, *FLORAL*
390 *TRANSITION AT THE MERISTEM1* (*FTM1*) (Torti et al., 2012), and *JUMONJI*
391 *DOMAIN-CONTAINING PROTEIN30* (*JMJ30*) (Jones et al., 2010; Yan et al., 2014)
392 (**Supplemental Data Set 4**). In addition, 39 genes differentially marked by both
393 H3K27me3 and H3K4me3 were detected, including the flowering-time regulators
394 *miR156D* and *AGL19* (**Supplemental Data Set 4, Figure 6C**).

395 We also examined the extent to which the differentially marked genes were
396 also differentially expressed. H3K27me3 is associated with gene repression, and
397 therefore, genes with higher H3K27me3 levels in *chr4*-2 compared to Col-0 were
398 expected to be expressed at lower levels in *chr4*-2 than in Col-0. Indeed, a significant
399 overrepresentation (Representation factor: 6.2, *p*-value < 1.317e-11) of
400 downregulated genes was observed among those marked with increased levels of

401 H3K27me3 in *chr4*-2 (**Figure 6B**). Among the downregulated and hypermethylated
402 genes in *chr4-2* was *AHL3*, encoding an AT-hook protein that regulates vascular
403 tissue boundaries in roots (Zhou et al., 2013) (**Figure 6C**). By contrast, H3K4me3 is
404 associated with gene activation and therefore, genes marked with higher H3K4me3
405 levels in *chr4*-2 compared to Col-0 were expected to be expressed at higher levels.
406 Indeed, a significant overrepresentation (Representation factor: 10.8, *p*-value <
407 2.176e-48) of upregulated genes between those marked with higher levels of
408 H3K4me3 was observed (**Figure 6B**). Among the upregulated and hypermethylated
409 genes in *chr4-2* are *CHR23*, which is involved in stem-cell maintenance at the SAM
410 (Sang et al., 2012) and *SPL15,* a promoter of the floral transition at the shoot
411 meristem (Hyun et al., 2016) (**Figure 6C**). Moreover, *spl15* produced fewer cauline
412 leaves than the wild type (Schwarz et al., 2008), indicating a premature transition to
413 the I_2 phase of flower initiation. On the other hand, plants expressing a miR156-
414 resistant transcript of *SPL15* (*rSPL15*), which leads to an increase in SPL15 protein
415 accumulation, produced more cauline leaves than the wild type (Hyun et al, 2016),
416 indicating a delay in the transition to the I_2 phase of flower initiation, as observed in
417 *qem2* mutants.
418 In conclusion, CHR4 affects H3K27me3 and H3K4me3 levels at a subset of
419 loci in the genome, and changes in both histone modifications in *chr4*-2 are
420 significantly correlated with changes in gene expression. Notably, a significant
421 increase in H3K4me3 was detected at the *SPL15* locus, and a higher level of *SPL15*
422 mRNA was found in *chr4*-2; these findings are consistent with the premature bolting
423 and delay in the transition to the I_2 phase of flower initiation observed in *chr4-2*.

424 **DISCUSSION**

425 We performed an enhanced genetic screen to identify regulators of the floral
426 transition, and in particular, to focus on endogenous flowering pathways at the shoot
427 meristem. To this end, we generated a quintuple mutant background strongly
428 impaired in floral responses to environmental stimuli. Mutagenesis of these plants
429 identified a chromatin remodeller, CHR4, which plays important roles in the floral
430 transition, especially in response to endogenous flowering pathways and during the
431 transition from forming cauline leaves with axillary branches (I_1) to forming floral
432 primordia (I_2).

433 **The quintuple mutant is strongly impaired in environmental flowering**
434 **responses and flowers via endogenous pathways**
435 The quintuple mutant showed strongly reduced flowering responses to long
436 photoperiods and high ambient temperature. This insensitivity is consistent with the
437 loss of function of *FT* and *TSF*, which confer photoperiodic responses, and the loss of
438 function of *FT, TSF* and *SVP*, which are involved in responses to high ambient
439 temperature (Yamaguchi et al., 2005; Kumar et al., 2012; Fernandez et al., 2016).
440 Therefore, the floral transition in the quintuple mutant is likely promoted by
441 endogenous flowering pathways. In support of this conclusion, RNA-seq analysis
442 detected higher mRNA levels of several *SPL* genes in the mutant vs. Col-0. Some of
443 these genes, such as *SPL15* and *SPL4*, are negatively regulated by miR156, which
444 decreases in abundance as plants proceed from the juvenile to the adult phase (Wu
445 and Poethig, 2006; Gandikota et al., 2007; Hyun et al., 2016). Therefore, these SPLs
446 were previously considered to be components of an age-related flowering pathway
447 (Wang et al., 2009; Hyun et al., 2017). However, the mRNA of *SPL8*, which is not
448 regulated by miR156 but has overlapping functions with the miR156-targeted *SPL*
449 genes (Xing et al., 2010), also increased in abundance in the quintuple mutant,
450 suggesting a broader deregulation of this class of transcription factors in this genetic
451 background.
452 Transcriptome profiling of the quintuple mutant also detected differential
453 expression of genes encoding enzymes involved in GA biosynthesis, such
454 as *GA20ox2*. Higher *GA20ox2* mRNA expression was detected in the quintuple
455 mutant compared to Col-0 under SDs. The accumulation of GA_4 under SDs in Col-0
456 plants coincides with the floral transition and increased abundance of the mRNAs of
457 floral meristem identity genes such as *LFY* (Eriksson et al., 2006). Although the GA
458 biosynthesis pathway is complex and includes many enzymatic steps (Yamaguchi,
459 2008), *GA20ox2* appears to be important for controlling the floral transition, especially
460 under SDs (Rieu et al., 2008; Plackett et al., 2012; Andres et al., 2014). SVP reduces
461 *GA20ox2* transcript levels and GA levels at the shoot apex as part of the mechanism
462 by which it represses flowering (Andres et al., 2014). We therefore propose that
463 increased *GA20ox2* transcription in the quintuple mutant contributes to its higher GA
464 levels and earlier floral transition under SDs. In support of this notion, the *qem1*
465 mutation was found to be an allele of *GA20ox2* and to delay flowering of the
466 quintuple mutant.

467 The proposed role for SPLs and GA in causing early flowering of the quintuple
468 mutant is consistent with the previous finding that SPL proteins mediate some of the
469 effects of GA during reproductive development (Porri et al., 2012; Yu et al., 2012;
470 Yamaguchi et al., 2014; Hyun et al., 2016) and that SPL8 regulates several GA-
471 mediated developmental processes (Zhang et al., 2007). Furthermore, SPL9 and
472 SPL15 interact with DELLA proteins, which are negative regulators of GA responses
473 that are degraded in the presence of GA (Daviere and Achard, 2013). SPL15
474 promotes the transcription of target genes that induce flowering, such as *FUL* and
475 *miR172b*, and activation of these genes by SPL15 is repressed by interaction with
476 DELLAs (Hyun et al., 2016). In Col-0, the role of SPL15 in flowering is particularly
477 important under SDs, when floral induction occurs independently of environmental
478 cues and is dependent on endogenous processes such as the GA pathway (Hyun et
479 al., 2019). By contrast, the DELLA-SPL9 interaction can negatively or positively affect
480 transcription, depending on the target genes and the developmental context
481 (Yamaguchi et al., 2009; Yu et al., 2012). Taken together, these results demonstrate
482 that the floral transition in the sensitized quintuple mutant background involves the
483 interdependent functions of GA and SPL proteins.

484 **A chromatin remodeller was identified as a regulator of the floral transition in**
485 **the sensitized screen**

486 The genetic framework for flowering-time control in Arabidopsis is based on analysis
487 of late-flowering mutants identified after mutagenesis of early-flowering accessions
488 (Koornneef et al., 1998). However, important regulators were not identified in these
489 screens, but were readily found as early-flowering mutants from mutagenising late-
490 flowering lines (Michaels and Amasino, 1999) or as late-flowering suppressor
491 mutants after mutagenesis of transgenic plants or mutants requiring vernalization
492 (Chandler et al., 1996; Onouchi et al., 2000). Here, we extended this approach by
493 mutagenising a quintuple mutant background that flowered almost independently of
494 environmental cues. Until recently, the molecular characterization of mutations
495 isolated in such complex backgrounds using classical genetic approaches would
496 have been extremely time-consuming and laborious, but this process has been
497 simplified by the implementation of bulk-segregant analysis after backcrossing the
498 mutant to the progenitor followed by whole-genome resequencing (Abe et al., 2012;
499 Hartwig et al., 2012; Schneeberger, 2014).

500 The second characterized mutation identified in the quintuple mutant
501 background, *qem2*, is an allele of *CHR4*. This gene encodes a chromatin remodeller
502 that was previously identified as a member of protein complexes that include AP1
503 and other MADS-box transcription factors (Smaczniak et al., 2012), but its role in
504 flowering had not been demonstrated genetically. Nevertheless, several chromatin
505 modifiers and remodellers contribute to the regulation of the floral transition (Farrona
506 et al., 2008), such as BRAHMA (BRM), a member of the SWI/SNF complex involved
507 in nucleosome sliding and/or eviction, and the H3K27me3-specific histone
508 demethylase RELATIVE OF EARLY FLOWERING6 (REF6), which acts cooperatively
509 with BRM to regulate gene expression during floral development (Farrona et al.,
510 2004; Lu et al., 2011; Wu et al., 2012; Li et al., 2016; Richter et al., 2019). Also, the
511 SWI2/SNF2-RELATED1 (SWR1) complex protein PHOTOPERIOD-INSENSITIVE
512 EARLY FLOWERING1 (PIE1) is involved in H2A.Z deposition and delays the floral
513 transition (Noh and Amasino, 2003; March-Diaz et al., 2008; Coleman-Derr and
514 Zilberman, 2012). Interestingly, PKL and PIE1 were previously proposed to act in the
515 same pathway to define and maintain genomic domains with elevated H3K27me3
516 levels, suggesting that CHR4 may contribute at different levels within this process
517 (Carter et al., 2018). Taken together, mass spectrometry identified several proteins in
518 association with CHR4 that are involved in regulating histone modifications as well as
519 multiple transcription factors with specific roles in floral meristem identity or the floral
520 transition, suggesting that CHR4 functions in different multimeric complexes that
521 regulate flowering.
522

523 **CHR4 affects the expression of flowering genes by modulating H3K4me3 and**
524 **H3K27me3 levels and affects different stages of the floral transition**

525 The most closely related protein to CHR4 is another CHD3-like family member, PKL,
526 which orchestrates deposition of H3K27me3 and facilitates nucleosome retention
527 (Zhang et al., 2008; Zhang et al., 2012; Jing et al., 2013; Carter et al., 2018). In rice,
528 loss of function of the CHR4 homologue CHR729 results in changes in the
529 abundance of H3K27me3 and H3K4me3 at approximately 56% and 23%,
530 respectively, of loci marked by these modifications (Hu et al., 2012). Similarly, we
531 observed variation in H3K27me3 or H3K4me3 levels at a subset of loci marked by
532 these modifications in *chr4*-2, indicating a conserved function between rice and

533 Arabidopsis. Notably, we observed higher levels of H3K4me3 at the *SPL15* locus in
534 *chr4*-2 vs. the wild type.

535 The floral transition is considered to be a dual-step process: in the first step,
536 the inflorescence meristem produces cauline leaves and axillary branches (I_1), and in
537 the second phase, it forms floral primordia (I_2) (Ratcliffe et al., 1999). Detailed
538 phenotypic analysis of *chr4* mutants showed that CHR4 affects both these phases
539 but with opposite effects. The *chr4* mutation accelerates the transition from the
540 vegetative meristem to I_1 but delays the I_1 to I_2 transition. The premature transition to
541 I_1 was reflected by earlier bolting, and this correlated with increased abundance of
542 *SPL15*, *SPL4* and *FUL* mRNA expression. These genes are associated with early
543 bolting and flowering, and *SPL15* in particular caused premature bolting when its
544 expression was increased by mutations that rendered its mRNA insensitive to
545 miR156 (Hyun et al., 2016). SPL15 also promotes the meristematic transition from
546 vegetative to inflorescence meristem (Hyun et al., 2016). Moreover, *spl15* mutants
547 produced fewer cauline leaves than the wild type (Schwarz et al., 2008), whereas
548 *rSPL15* transgenic plants produced more cauline leaves (Hyun et al., 2016),
549 indicating that SPL15 extends the I_1 phase. We propose that the higher expression of
550 *SPL15* in *chr4* promotes earlier bolting and extends the I_1 phase. This increased
551 activity of SPL15 could also be enhanced in *chr4* by increased activity of the GA
552 biosynthetic pathway, as the resulting reduction in DELLA activity would be predicted
553 to allow SPL15 to more effectively activate transcription of its target genes, leading to
554 premature bolting and more cauline leaves.

555 Mutant *chr4* plants also produced more cauline leaves and required more time
556 to open the first flowers than their progenitors, indicating a delay in the I_2 transition.
557 These mutants also exhibited higher levels of *TFL1* and *BFT* mRNAs; the
558 overexpression of these genes delays the I_2 transition by repressing *AP1* and *LFY*
559 expression (Ratcliffe et al., 1998; Yoo et al., 2010). Consistent with this conclusion,
560 the onset of *AP1* transcription occurred later in *qem2* than in the quintuple mutant
561 progenitor, and *LFY* mRNA was less abundant in *qem2* than in the quintuple mutant
562 in the RNA-seq time-course at week 6 in SDs. The *chr4* mutant phenotype is strongly
563 enhanced in the quintuple mutant background, probably explaining why *chr4* was
564 recovered in the sensitized mutant screen but was not previously identified by
565 mutagenesis of Col-0 plants, where it exhibited a strong effect only under SDs. We

566 propose that CHR4 contributes to the floral transition in response to GA signalling
567 and that the increased dependency of the quintuple mutant on the GA pathway to
568 promote flowering increases the impact of *CHR4* loss of function on the floral
569 transition. Similarly, the stronger phenotype of *chr4-2* in Col-0 under SDs than LDs is
570 consistent with a specific role in the floral transition mediated by GA.

571 In conclusion, the combination of forward genetics and functional gene
572 characterization identified CHR4 as a regulator of different stages of the floral
573 transition. Immunoprecipitation of CHR4 suggested that it acts in distinct protein
574 complexes that contain different transcription factors as well as other chromatin
575 remodelling proteins. The contribution of CHR4 within distinct complexes presumably
576 explains its pleiotropic effects, even during flowering, where it affects both bolting and
577 floral identity during the transition from I_1 to I_2. Our genome-wide analyses represent
578 the first step in understanding the mechanism by which CHR4 affects these
579 phenotypes by identifying genes whose expression is altered by H3K27me3 or
580 H3K4me3 in *chr4* mutants. Further studies are now required to link the specific
581 protein complexes in which CHR4 contributes to histone changes on defined targets.
582 Attempts to perform ChIP-seq on *pCHR4:CHR4-VENUS* lines did not succeed, but
583 pursuing this approach in the future would define the genome-wide sites with which
584 CHR4 associates and help define its effects on the histone marks at direct target
585 genes. Such approaches would help determine the mechanisms by which CHR4
586 regulates gene expression and allow this mechanism to be compared with that of
587 PKL, which cooperates with PIE1 and CLF at target genes to maintain elevated
588 H3K27me3 levels (Carter et al., 2018).

589

590 **METHODS**

591 **Plant materials, growth conditions, and phenotypic analysis**

592 For all studies, *Arabidopsis thaliana* Columbia (Col-0) ecotype was used as the wild
593 type (WT). To construct the *svp-41 flc-3 ft-10 tsf-1 soc1-2* quintuple mutant, *svp-41*
594 *flc-3 FRI* plants (Mateos et al., 2015) were first crossed to *svp-41 ft-10 tsf-1 soc1-2*
595 *ful-2* plants (Andres et al., 2014). The F_1 plants were self-fertilized and the F_2
596 progeny were genotyped for each mutation except *ful-2*, which was scored
597 phenotypically. Approximately 1,000 F_2 plants were grown in soil under LD conditions
598 and DNA was extracted from those that flowered later than Col-0. Genotyping was

599 performed to identify plants that carried all mutations, lacked the *FRI* introgression,
600 and were homozygous for *FUL* in the F_3 generation. *chr4*-2 corresponds to
601 SAIL_783_C05. Homozygous mutant plants were selected by PCR using specific
602 primers (**Supplemental Data Set 5**).

603 Seeds were immersed in 0.1% melt universal agarose (Bio-Budget
604 Technologies GmbH) for three days at 4°C in darkness for stratification. Plants were
605 grown in soil under controlled conditions of LDs (16 h light/8 h dark) and SDs (8 h
606 light/16 h dark) at 21°C or 27°C. The light intensity was 150 $\mu mol \cdot m^{-2} \cdot s^{-1}$ under all
607 conditions. The growth-chamber is equipped with fluorescent tube bulbs from Philips
608 (F17T8/TL841 ALTO-T8) to supply wavelengths from 430 to 650 nm, and
609 supplemented with LEDs to provide light in the far-red spectrum. As a proxy for
610 flowering time, the number of rosette and cauline leaves on the main shoot was
611 counted as well as the number of days to bolting and first flower opening.

612 **Ethylmethanesulfonate (EMS) treatment of seeds**

613 For EMS treatment, 200 mg (~10,000) seeds of the quintuple mutant were wrapped
614 in Miracloth and immersed in 0.1% KCl solution on a shaker at 4°C for 14 h. The
615 seeds were washed with ddH_2O and treated with 100 mL 30 mM EMS diluted in
616 ddH_2O on a magnetic stirrer in a fume hood overnight (8–9 h). The seeds were
617 washed twice with 100 mL 100 mM sodium thiosulfate for 15 min and three times
618 with 500 mL ddH_2O for 30 min. After washing, the seeds were immersed in 2 L 0.1%
619 agarose. Approximately 50 seeds in 10 mL agarose were sown as the M_1 generation
620 in 9 × 9 cm pots using plastic pipettes. The M_1 plants were grown and self-fertilized,
621 and seeds were harvested in bulks of 50 M_1 plants. One hundred and forty-six M_2
622 bulked families were screened for plants showing altered flowering time.

623 **GA treatment**

624 The GA_4 stock (Sigma, Cat. G7276-5MG) was prepared in 100% ethanol with a final
625 concentration of 1 mM. GA treatments were performed by spraying 2-week-old plants
626 under SDs with either a GA solution (10 μM GA_4, 0.02% Silwet 77) or a mock solution
627 (1% ethanol, 0.02% Silwet 77). Spraying was performed twice weekly until the plants
628 bolted.

629 **Selection of mutants and sequencing**

630 Approximately 10 M_2 generation seeds from each M_1 plant were sown. Screening for
631 potential mutants was initially performed under LD greenhouse conditions, and all
632 plants were grown together with the quintuple mutant and Col-0 plants as a
633 reference. Individuals that flowered later or earlier than the quintuple mutant in the M_2
634 population were selected. These M_2 putative mutants were self-fertilized and
635 rescreened in the M_3 generation. Approximately 24 M_3 progeny of each potential
636 mutant were grown under the same conditions to test the heritability of the
637 phenotype. M_3 plants were backcrossed to the quintuple mutants to generate $BC1F_1$
638 seeds. The $BC1F_2$ offspring of such a cross formed the isogenic mapping population.
639 Approximately 70 plants showing the mutant phenotype were selected from a
640 population of ~300 $BC1F_2$ plants. One leaf sample of each selected plant was
641 harvested and pooled. Leaf material from the quintuple plants was also harvested as
642 a control. Genomic DNA was extracted from both pools and sent for Illumina
643 sequencing with a depth of approximately 80-fold coverage. Reads were aligned to
644 the TAIR10 reference genome using SHORE (Schneeberger et al., 2009).
645 SHOREmap (Schneeberger et al., 2009; Sun and Schneeberger, 2015) was used to
646 identify polymorphisms, and those present in approximately 100% of reads in the
647 identified mutant but absent from the progenitor were identified as candidates for the
648 causal mutation.

649 ***In situ* hybridization**

650 *In situ* hybridization was performed as previously described (Bradley et al., 1993),
651 with minor modifications. Instead of Pronase, proteinase K (1 mg/mL in 100 mM Tris,
652 pH 8, and 50 mM EDTA) was used for protease treatment by incubating at 37°C for
653 30 min. Post-hybridization washes were performed in 0.1× SSC instead of the
654 original 2× SSC with 50% formamide. The sequences of primers used to generate
655 the probes are listed in **Supplemental Data Set 5**. For each genotype and time point,
656 3 independent apices were analyzed.

657 **RNA extraction and RNA-seq analysis**

658 Total RNA was extracted from 15 shoot apices after removing all visible leaves under
659 a binocular for each of the three independent biological replicates using an RNeasy
660 Plant Mini Kit (Qiagen) and treated with DNase (Ambion) to remove residual genomic
661 DNA. Library for sequencing was prepared using an Illumina TruSeq library
662 preparation kit according to the manufacturer's protocol. Sequencing was performed

663 using Illumina the HiSeq3000 platform in 150-bp single reads. For each sample,
664 approximatively 15,000,000 reads were generated. FastQC was used to assess
665 quality control parameters
666 (https://www.bioinformatics.babraham.ac.uk/projects/fastqc/). To estimate expression
667 levels, the RNA-seq reads were mapped to the *A. thaliana* TAIR10 (Lamesch et al.,
668 2012) reference genome (ftp://ftp.arabidopsis.org/home/tair) using TopHat2 under
669 default settings (Kim et al., 2013), except that only a single alignment was permitted
670 per read and the coverage-based junction search was disabled (settings: -g 1 –no-
671 coverage-search). Samtools was used to sort and index BAM alignment files and to
672 calculate BAM file statistics (Li et al., 2009). HTSeq was used to tabulate the number
673 of reads mapping to each genomic feature, with counts tabulated only for genes that
674 completely overlapped a given feature (Anders et al., 2015). We used the Wald test
675 implemented in DESeq2 to detect differentially expressed genes for pair-wised
676 comparison. To visualise the expression levels of candidate genes, the expression
677 level for each gene was calculated as transcripts per million (TPM).

678 **ChIP-seq experiment and data analysis**

679 Three independent biological replicates for each genotype were generated. For each
680 sample, 1 g plant material was used per biological replicate. Material was collected
681 from plants grown in SD at 21°C for 5 weeks (5–6 h after lights on). Using jeweler's
682 forceps, leaves with elongated petioles were removed to obtain SAM-enriched
683 tissues. ChIP experiments were performed following a previously published protocol
684 (Kaufmann et al., 2010) with minor modifications. Samples were sonicated in a water
685 bath Bioruptor (Diagenode) four times for 5 min each of 15 sec on and 15 sec off,
686 with a 1-min incubation between each sonication treatment. After the preclearing
687 step, the sample was split into three aliquots: the first aliquot was incubated with anti-
688 H3K27me3 antibody (Active Motif, Cat. 39155, Lot. 25812014), the second one was
689 incubated with anti-H3K4me3 antibody (Millipore, Cat.17–614, Lot.1973237) and the
690 third one with anti-H3 antibody (ab1791, Abcam). Samples were prepared for Illumina
691 sequencing using the Ovation Ultralow V2 DNA-Seq Library Preparation Kit from
692 Tecan Genomics according to the manufacturer's protocol. H3K27me3 and
693 H3K4me3 enrichment was tested by ChIP-qPCR before and after library preparation.
694 Libraries were analyzed on the Bioanalyzer and quantified with the qBit before
695 sequencing on the HiSeq3000. Samples were sequenced in a 150-bp single reads
696 run.

697 FASTQ files were mapped to the *A. thaliana* genome TAIR10 using Bowtie
698 (Langmead et al., 2009) with default parameters. Clonal reads were removed using a
699 customised python script. Reproducibility between biological replicates was assessed
700 using the Spearman correlation for the genome-wide read distribution at each pair of
701 replicates using DeepTool (Ramirez et al., 2014). The "multiBamSummary" function
702 was used with default parameters except for "bin size", which was set to 1 kb and the
703 "plotCorrelation" function of deepTools2 in Galaxy (http://deeptools.ie-
704 freiburg.mpg.de/) (**Supplemental Figure 9**). H3K27me3 and H3K4me3 modified
705 regions were identified with DANPOS2 (Chen et al., 2013). The "Dpeak" function in
706 DANPOS2 was used with default parameters, except for the parameter – l (read
707 extension length), which was set to 300 bp, the mean size of the DNA in the samples
708 after sonification. Genomic regions were associated with genes if located within the
709 start and the end of the gene using a customised python script.

710 **Plasmid construction**

711 Cloning of the *CHR4* locus was performed based on polymerase incomplete primer
712 extension (Klock and Lesley, 2009) with modifications for large fragments and
713 multiple inserts. All PCR amplifications were performed with Phusion Enzyme (New
714 England BioLabs) following the manufacturer's recommendations. The constructs
715 pCHR4:CHR4-pDONR207 (18.4 kb) and pCHR4:CHR4:9AV-pDONR207 (19 kb)
716 were generated as follows. Primers Q810 and Q811 were used to amplify the *CHR4*
717 promoter (3.6 kb) and the PCR products were cloned into pDONR207 by BP reaction
718 to generate the pCHR4-pDONR207 construct. The primer pairs Q058 and Q814, and
719 Q815 and Q816 were used to amplify a fragment containing 9xala-VENUS (9AV) (0.7
720 kb) and the 3´UTR of CHR4 (3.8 kb), respectively. Overlap PCR with primers Q058
721 and Q816 was performed to fuse the amplicons. The primers Q817 and Q818 were
722 used to linearize the construct pCHR4-pDONR207. The amplicons were mixed with
723 linearized pCHR4-pDONR207 to construct the plasmid pCHR4:9AV:3'URTCHR4-
724 pDONR207. The obtained plasmid was linearized with primers Q835 and Q836 and
725 mixed with the coding sequence of *CHR4* (8.5 kb) amplified with primers Q819 and
726 Q820 to construct the plasmid pCHR4:CHR4:9AV-pDONR207 (called *pCHR4:CHR4-*
727 *VENUS* in the text). All primers used for molecular cloning are listed in
728 **Supplemental Data Set 5**. Subsequently, the plasmids were cloned into the binary
729 vector pEarleyGate301 (Earley et al., 2006) by LR reaction and transformed into *E.*

730 *coli* DH5-α-cells before being transformed into *Agrobacterium tumefaciens* GV3101
731 cells (Van Larebeke et al., 1974).

732 **Plant transformation and selection**

733 Plants (Col-0 and *svp flc ft tsf soc1*) were transformed by the floral-dip method
734 (Clough and Bent, 1998). Transformants were selected by spraying twice with
735 BASTA. The progenies were grown on plates with 1× Murashige and Skoog (MS)
736 medium (Murashige and Skoog, 1962) containing sucrose and 10 µg mL^{-1}
737 phosphinotricin (PPT) to test for segregation and to select for single locus insertion
738 lines and homozygosity in the following generations. Alternatively, the nondestructive
739 ppt leaf assay was used to assess resistance to PPT. One young leaf per plant was
740 harvested and placed on a plate with 1 MS without sucrose with 10 µg mL^{-1} PPT. The
741 plates were incubated for four days.

742 **Confocal microscopic analyses**

743 To visualise VENUS expression in shoot meristems, the method of (Kurihara et al.,
744 2015) was used with minor modifications. Shoot apices were collected and placed in
745 ice-cold 4% paraformaldehyde (PFA; Sigma-Aldrich) prepared in phosphate-buffered
746 saline (PBS) at pH 7.0. The samples were vacuum infiltrated twice for 10 min each
747 time, transferred to fresh 4% PFA, and stored at 4°C overnight. The next day, the
748 samples were washed in PBS twice for 10 min each and cleared with ClearSee (10%
749 xylitol, 15% sodium deoxycholate and 25% urea) at room temperature for ~1 week.
750 The samples were then transferred to fresh ClearSee solution with 0.1%
751 Renaissance 2200 and incubated in the dark overnight. The shoot meristems were
752 imaged by confocal laser scanning microscopy (Zeiss LSM780) using settings
753 optimised to visualise VENUS fluorescent proteins (laser wavelength, 514 nm;
754 detection wavelength, 517–569 nm) and Renaissance 2200 (laser wavelength, 405
755 nm; detection wavelength, 410–510 nm).

756 **Sample preparation and LC-MS/MS data acquisition**

757 Three independent biological replicates for each genotype (gCHR4-VENUS and
758 p35S-YFP), each consisting of 1 g plant material were generated. For inflorescence
759 tissues, plants were grown in LD at 21°C, whereas SAM-enriched tissue samples
760 were collected from plants growing in SD at 21°C for 5 weeks (5–6 h after lights on).
761 Using jeweler's forceps, leaves with elongated petioles were removed to obtain SAM-

762 enriched tissues. Nuclei were isolated according to a published protocol (Kaufmann
763 et al., 2010). Samples were sonicated in a Bioruptor (Diagenode) water bath four
764 times, 5 min each of 15 sec on and 15 sec off, with a 1-min incubation between each
765 sonication treatment. Sonicated samples were centrifuged twice at 4°C for 10 min.
766 The supernatants were transferred to a clean tube. After adding 40 µL GFP-trap
767 Agarose beads from Chromotek (gta-20) and 10 µL Benzonase, the samples were
768 incubated at 4°C for 2 hr. After incubation, the GFP-trap beads were washed four
769 times with 1 mL wash buffer (750 µL 5M NaCl, 1.25 mL Tris-HCl pH 7.4 in 25 mL
770 H_2O). Immunoprecipitated samples enriched with GFP-trap beads were submitted to
771 on-bead digestion. In brief, dry beads were re-dissolved in 25 µL digestion buffer 1
772 (50 mM Tris, pH 7.5, 2M urea, 1 mM DTT, 5 µg μL^{-1} trypsin) and incubated for 30 min
773 at 30°C in a Thermomixer with 400 rpm. Next, the beads were pelleted and the
774 supernatant was transferred to a fresh tube. Digestion buffer 2 (50 mM Tris, pH 7.5,
775 2M urea, 5 mM CAA) was added to the beads. After mixing and centrifugation, the
776 supernatant was collected and combined with the previous one. The combined
777 supernatants were incubated overnight in the dark at 32°C in a Thermomixer at 400
778 rpm. The digestion was stopped by adding 1 µL trifluoroacetic acid (TFA) and the
779 samples were desalted with C18 Empore disk membranes according to the StageTip
780 protocol (Rappsilber et al., 2003).
781 Dried peptides were re-dissolved in 2% acetonitrile (ACN), 0.1% TFA (10 µL)
782 for analysis and measured without dilution. The samples were analyzed using an
783 EASY-nLC 1200 (Thermo Fisher) coupled to a Q Exactive Plus mass spectrometer
784 (Thermo Fisher). Peptides were separated on 16-cm frit-less silica emitters (New
785 Objective, 0.75 µm inner diameter), packed in-house with reversed-phase ReproSil-
786 Pur C18 AQ 1.9 µm resin (Dr. Maisch). Peptides (0.5 µg) were loaded onto the
787 column and eluted for 115 min using a segmented linear gradient of 5% to 95%
788 solvent B (0 min: 5%B; 0–5 min -> 5%B; 5–65 min -> 20%B; 65–90 min ->35%B; 90–
789 100 min -> 55%; 100–105 min ->95%, 105–115 min ->95%) (solvent A 0% ACN,
790 0.1% FA; solvent B 80% ACN, 0.1%FA) at a flow rate of 300 nL min^{-1}. Mass spectra
791 were acquired in data-dependent acquisition mode using the TOP15 method. MS
792 spectra were acquired in the Orbitrap analyzer with a mass range of 300–1750 m/z at
793 a resolution of 70,000 FWHM and a target value of 3×10^6 ions. Precursors were
794 selected with an isolation window of 1.3 m/z. HCD fragmentation was performed at a
795 normalized collision energy of 25. MS/MS spectra were acquired with a target value

796 of 10^5 ions at a resolution of 17,500 FWHM, a maximum injection time of 55 ms, and
797 a fixed first mass of m/z 100. Peptides with a charge of +1, greater than 6, or with an
798 unassigned charge state were excluded from fragmentation for MS2. Dynamic
799 exclusion for 30s prevented repeated selection of precursors.

800 **Data analysis**

801 Raw data were processed using MaxQuant software (version 1.5.7.4,
802 http://www.maxquant.org/) (Cox and Mann, 2008) with label-free quantification (LFQ)
803 and iBAQ enabled (Tyanova et al., 2016). MS/MS spectra were searched by the
804 Andromeda search engine against a combined database containing *A. thaliana*
805 sequences (TAIR10_pep_20101214; ftp://ftp.arabidopsis.org/home/tair/Proteins/
806 TAIR10_protein_lists/) and sequences of 248 common contaminant proteins and
807 decoy sequences. Trypsin specificity was required and a maximum of two missed
808 cleavages allowed. Minimal peptide length was set to seven amino acids.
809 Carbamidomethylation of cysteine residues was set as fixed and oxidation of
810 methionine and protein N-terminal acetylation as variable modifications. Peptide-
811 spectrum-matches and proteins were retained if they were below a false discovery
812 rate of 1%. Statistical analysis of the MaxLFQ values was carried out using Perseus
813 (version 1.5.8.5, http://www.maxquant.org/). Quantified proteins were filtered for
814 reverse hits and hits "identified by site", and MaxLFQ values were $\log_2$-transformed.
815 After grouping the samples by condition, only proteins that had two valid values in
816 one of the conditions were retained for subsequent analysis. Two-sample *t*-tests were
817 performed with a permutation-based FDR of 5%. Alternatively, quantified proteins
818 were grouped by condition and only hits that had three valid values in one of the
819 conditions were retained. Missing values were imputed from a normal distribution (0.3
820 width, 2.0 downshift, separately for each column). Volcano plots were generated in
821 Perseus using an FDR of 1% and an S0 = 1. The Perseus output was exported and
822 further processed using Excel. ANOVA tables are shown in **Supplemental Data Set**
823 **6.**
824

825 **Accession Numbers**

826 The sequence of the genes and loci described here can be obtained from TAIR using
827 the following gene identifiers: CHR4 (AT5G44800), SVP (AT2G22540), FLC
828 (AT5G10140), SOC1 (AT2G45660), FT (AT1G65480), TSF (AT4G20370), GA20ox2
829 (AT5G51810) and SPL15 (AT3G57920).

830

831 The Illumina sequencing data have been deposited to the GEO with the dataset
832 identifier GSE140728. The mass spectrometry proteomics data have been deposited
833 to the ProteomeXchange Consortium via the PRIDE (Vizcaino et al., 2016) partner
834 repository with the dataset identifier PXD016457.

835

836 **Supplemental Data**

837 **Supplemental Figure 1**. svp flc ft tsf soc1 probably flowers as a result of
838 endogenous pathways.
839 **Supplemental Figure 2**. Molecular genetic analysis of *qem1*.
840 **Supplemental Figure 3.** *CHR4* expression in Col-0 and *chr4-2*.
841 **Supplemental Figure 4.** *CHR4* loss-of-function phenotype in LDs.
842 **Supplemental Figure 5.** Shoot apical meristem size.
843 **Supplemental Figure 6.** CHR4 expression profile and protein localization.
844 **Supplemental Figure 7.** Volcano plot of protein–protein interactions.
845 **Supplemental Figure 8.** Global accumulation H3K27me3 and H3K4me3 marks in
846 Col-0 and *chr4-2*.
847 **Supplemental Figure 9.** Spearman correlation for ChIP-seq samples.
848 **Supplemental Table 1.** Candidate SNPs annotated in genes by SHOREmap for
849 *qem1*.
850 **Supplemental Data Set 1.** Whole-genome expression profiling experiments
851 comparing the profiles of the genotypes Col-0 and *svp flc ft tsf soc1* grown for 3, 4, 5
852 or 6 weeks under SD conditions.
853 **Supplemental Data Set 2.** Whole-genome expression profiling experiments
854 comparing the profiles of the genotypes Col-0 vs *chr4-2* and *svp flc ft tsf soc1* vs.
855 *qem2* grown for 3, 4, 5 or 6 weeks under SD conditions.
856 **Supplemental Data Set 3.** IP-MS results for CHR4-VENUS and AP1-GFP pull-down:
857 list of CHR4-interacting proteins.
858 **Supplemental Data Set 4.** Comparative analysis of H3K27me3 and H3K4me3 ChIP-
859 seq results in Col-0 and *chr4*-2 obtained with DANPOS2.
860 **Supplemental Data Set 5.** List of primers used in the study.
861 **Supplemental Data Set 6.** ANOVA tables.
862

863

864

865 **Table 1.** Candidate SNPs in *qem2* annotated in genes.

Chr[1]	Pos[2]	R[3]	M[4]	N[5]	AF[6]	Sh[7]	Region[8]	Gene ID[9]	Type[10]	AR[11]	AM[12]	Name
5	16,021,261	C	T	60	0.87	40	CDS	*At5g40010*	Nonsyn	G	S	*ASD*
5	17,457,889	C	T	38	1	40	CDS	*At5g43450*	Nonsyn	D	N	
5	18,031,708	G	A	27	1	40	CDS	*At5g44690*	Nonsyn	R	STOP	
5	18,089,069	G	A	52	1	40	CDS	*At5g44800*	Nonsyn	A	V	*CHR4*
5	19,281,739	G	A	40	0.93	40	CDS	*At5g47530*	Nonsyn	G	E	
5	19,572,635	G	A	17	0.94	32	3'UTR	*At5g48300*				*ADG1*
5	19,637,792	G	A	43	0.96	40	CDS	*At5g48460*	Nonsyn	A	V	*ATFIM2*
5	20,946,101	G	A	49	0.83	40	CDS	*At5g51560*	Nonsyn	G	S	

866

867 [1] Chr: chromosome. [2] Position: position of the mutated nucleotide. [3] R: nucleotide in the reference genome (*svp*
868 *flc ft tsf soc1*). [4] M: nucleotide in *qem2*. [5] N: number of reads supporting the mutation. [6] AF: allele frequency. [7] Sh:
869 SHORE Score (max. 40). [8] Region: region of the locus where the mutation was identified. [9] Gen ID: gene
870 identifier. [10] Type: type of mutation (nonsynonymous or synonymous). [11] AR: amino acid in the reference genome
871 (*svp flc ft tsf soc1*). [12] AM: amino acid in*qem2*.

Table 2. List of CHR4 interacting proteins.		**SAMs with younger leaves at 5w-SD-stage**			
Gene ID	Name	No. Of Unique Peptides (IP1-IP2-IP3)	Sequence Coverage (%) (IP1-IP2-IP3)	log2 ratio	p-value
AT5G44800	CHR4	142 (128-130-114)	59.6 (55.2-55.9-53.7)	10.41	1.43E-05
TRANSCRIPTION FACTORS					
AT1G69120	AP1	-	-	-	-
AT5G20240	PI	-	-	-	-
AT3G54340	AP3	-	-	-	-
AT5G15800	SEP1	-	-	-	-
AT3G02310	SEP2	-	-	-	-
AT2G45650	AGL6	-	-	-	-
AT2G42830	SHP2	-	-	-	-
AT3G13960	GRF5	7 (6-5-4)	18.1 (15.9-13.9-9.6)	6.05	2.16E-04
AT4G37740	GRF2	6 (6-5-3)	17.4 (17.4-15.3-9.5)	5.19	1.90E-05
AT5G43270	SPL2	-	-	-	-
AT1G02065	SPL8	-	-	-	-
AT1G27360	SPL11	-	-	-	-
AT5G50670	SPL13	5 (5-4-2)	19.2 (19.2-15-6.7)	4.84	2.20E-03
AT2G28550	TOE1	5 (5-5-3)	15.4 (15.4-15.4-8.7)	4.01	1.89E-03
AT3G02150	TCP13	5 (4-4-3)	18 (18-18-10.4)	4.21	2.20E-02
CHROMATIN REMODELLER					
AT2G46020	BRM	37 (30-31-16)	24.2 (19.3-19.7-10.8)	2.68	8.95E-04
AT1G08600	ATRX	23 (19-22-6)	13.9 (11.7-13.3-5.5)	5.23	9.14E-05
AT5G04240	ELF6	10 (8-10-1)	11.7 (7.8-11.7-0.8)	3.09	2.20E-03
AT2G28290	SYD	27 (21-21-15)	11.1 (7.9-7.9-5.9)	3.09	1.19E-03
AT2G25170	PKL	19 (17-17-14)	19.8 (16.7-17.4-14.8)	2.71	5.48E-04
AT3G12810	PIE1	18 (14-15-9)	11.5 (9.9-9.8-6.8)	3.23	6.26E-03
AT5G18620	CHR17	17 (15-15-8)	44.1 (42.4-42.4-25.3)	2.85	5.34E-04
AT3G06400	CHR11	12 (11-10-10)	45.1 (41.9-41.7-30.3)	2.90	6.86E-04
AT3G48430	REF6	27 (22-25-18)	23.4 (18.8-21-17)	2.92	2.49E-03

AT5G11530	EMF1	10 (7-8-3)	10.4 (6.9-8.3-3.5)	5.12	1.12E-04
AT2G06210	ELF8	14 (12-13-9)	15.9 (11.8-13.6-11.2)	2.72	2.50E-03
AT5G53430	SDG29	5 (4-5-2)	8 (7-8-4.5)	4.40	8.19E-03
AT4G02020	SWN	3 (2-1-2)	4.8 (3-1.3-3)	2.40	5.04E-03
General transcriptional coregulators					
AT3G07780	OBE1	14 (13-13-8)	31.3 (29.7-31.3-20.8)	6.47	7.02E-05
AT5G48160	OBE2	23 (21-17-9)	41.5 (40.8-30.1-19.3)	5.16	3.03E-03
AT1G15750	TPL	12 (11-10-9)	31.7 (27-26.9-24.4)	3.93	3.17E-04
AT1G80490	TPR1	9 (8-7-6)	25.4 (23.6-22.5-17.5)	4.59	2.03E-03
AT3G16830	TPR2	8 (7-6-4)	13.5 (12.6-10.2-5.1)	3.57	1.99E-02
AT2G32950	COP1	7 (6-7-2)	12.7 (11.7-12.7-4.3)	3.99	4.02E-03
AT2G46340	SPA1	10 (7-10-3)	13.2 (9.2-13.2-3.6)	2.72	3.80E-02
AT1G43850	SEU	12 (11-10-6)	18.1 (16.9-12.9-9.9)	3.69	2.49E-03
		Inflorescence under LDs			
Gene ID	Name	No. Of Unique Peptides (IP1-IP2-IP3)	Sequence Coverage (%) (IP1-IP2-IP3)	log2 ratio	p-value
AT5G44800	CHR4	117 (114-99-114)	51.4 (51.4-49.7-51.2)	8.76	1.09E-04
TRANSCRIPTION FACTORS					
AT1G69120	AP1	12 (8-3-7)	34 (21.5-10.2-24.2)	3.55	1.24E-02
AT5G20240	PI	8 (6-3-8)	31.7 (25.5-11.5-31.7)	6.31	3.36E-03
AT3G54340	AP3	7 (7-5-7)	31.5 (31.5-19-31.5)	4.56	4.63E-02
AT5G15800	SEP1	2 (2-1-2)	23.5 (23.5-17.1-21.9)	4.06	2.63E-02
AT3G02310	SEP2	3 (2-1-2)	32.8 (23.6-17.2-22)	4.05	4.47E-03
AT2G45650	AGL6	3 (3-2-3)	10.3 (10.3-10.3-10.3)	3.78	9.16E-03
AT2G42830	SHP2	4 (4-3-4)	29.3 (29.3-24-29.3)	4.88	6.01E-03
AT3G13960	GRF5	4 (3-3-4)	13.6 (9.1-9.1-13.6)	3.62	3.28E-02
AT4G37740	GRF2	1 (1-1-1)	3.2 (3.2-3.2-3.2)	1.39	2.17E-01
AT5G43270	SPL2	4 (4-4-4)	17.2 (17.2-17.2-17.2)	5.30	3.32E-03
AT1G02065	SPL8	4 (4-2-4)	18.3 (18.3-12-18.3)	3.93	1.40E-02
AT1G27360	SPL11	8 (5-2-7)	27 (17.8-10.2-21.9)	5.57	1.53E-03
AT5G50670	SPL13	4 (3-1-4)	13.9 (11.1-3.1-13.9)	3.68	4.96E-03
AT2G28550	TOE1	-	-	-	-
AT3G02150	TCP13	6 (5-3-5)	18.3 (15.5-10.1-15.5)	3.96	5.85E-03
CHROMATIN REMODELLER					
AT2G46020	BRM	24 (13-12-18)	13 (8.6-8.4-10)	2.57	2.36E-02
AT1G08600	ATRX	28 (20-18-24)	18.3 (13.8-13.3-16.3)	4.64	2.59E-03
AT5G04240	ELF6	4 (4-1-4)	5.8 (5.8-0.7-5.8)	2.63	5.22E-02
AT2G28290	SYD	21 (19-12-20)	8 (7.6-4.6-8)	3.70	4.76E-02
AT2G25170	PKL	26 (23-18-24)	23.6 (23-17.4-20.9)	3.49	1.38E-02
AT3G12810	PIE1	7 (4-3-6)	4.5 (3.2-2.6-4.1)	1.89	1.04E-01
AT5G18620	CHR17	14 (11-13-12)	37.4 (35.6-32.6-37.2)	2.97	1.49E-02
AT3G06400	CHR11	17 (13-9-14)	41.3 (39.2-32-39.1)	2.34	9.72E-03
AT3G48430	REF6	33 (27-17-29)	28.8 (24.8-12.9-24.5)	2.21	1.39E-02
AT5G11530	EMF1	7 (6-3-7)	8.5 (7.8-2.9-8.5)	3.31	1.96E-02
AT2G06210	ELF8	-	-	-	-
AT5G53430	SDG29	7 (4-1-5)	10.6 (7-2.5-7.2)	1.99	3.08E-02
AT4G02020	SWN	3 (2-2-2)	4.2 (2.5-2.5-2.5)	1.52	3.13E-02
General transcriptional coregulators					
AT3G07780	OBE1	12 (7-6-8)	26 (17.8-14.7-20.7)	4.12	3.47E-03
AT5G48160	OBE2	11 (9-5-11)	26.3 (21.3-12.9-26.3)	3.73	6.56E-03
AT1G15750	TPL	-	-	-	-
AT1G80490	TPR1	-	-	-	-
AT3G16830	TPR2	-	-	-	-
AT2G32950	COP1	4 (3-3-3)	6.7 (5.6-5.6-5.6)	1.17	1.63E-01
AT2G46340	SPA1	3 (1-1-2)	4.4 (1.4-1.4-2.6)	1.75	9.65E-03
AT1G43850	SEU	7 (6-2-6)	9.8 (9.7-3.6-8.6)	3.55	2.64E-03

872

ACKNOWLEDGEMENTS

We thank Anne Harzen for support in the mass-spectrometry experiments. We thank René Richter, Franziska Turck and John Chandler for critical comments to the manuscript. A.P. was supported by an EMBO long-term fellowship (AFL-2017-74). X. Y. was supported by the China Scholarship Council (201804910196). The laboratory of G.C. is funded by the Deutsche Forschungsgemeinschaft (DFG, German Research Foundation) under Germany´s Excellence Strategy (EXC 2048/1 Project ID: 390686111) and is supported by a core grant from the Max Planck Society.

AUTHOR CONTRIBUTIONS

S.Q., A.P. and G.C. conceived and designed the experiments. S.Q., A.P., X.Y. and F.A. performed the experiments. S.Q, A.P., K.S., H.S., B.S., S.S. and H.N. analysed the data. A.P, Q.S., and G.C wrote the manuscript.

REFERENCES

Abe, A., Kosugi, S., Yoshida, K., Natsume, S., Takagi, H., Kanzaki, H., Matsumura, H., Yoshida, K., Mitsuoka, C., Tamiru, M., Innan, H., Cano, L., Kamoun, S., and Terauchi, R. (2012). Genome sequencing reveals agronomically important loci in rice using MutMap. Nat Biotechnol **30,** 174-178.

Abe, M., Kosaka, S., Shibuta, M., Nagata, K., Uemura, T., Nakano, A., and Kaya, H. (2019). Transient activity of the florigen complex during the floral transition in Arabidopsis thaliana. Development **146**.

Abe, M., Kobayashi, Y., Yamamoto, S., Daimon, Y., Yamaguchi, A., Ikeda, Y., Ichinoki, H., Notaguchi, M., Goto, K., and Araki, T. (2005). FD, a bZIP protein mediating signals from the floral pathway integrator FT at the shoot apex. Science **309,** 1052-1056.

Aichinger, E., Villar, C.B., Farrona, S., Reyes, J.C., Hennig, L., and Kohler, C. (2009). CHD3 proteins and polycomb group proteins antagonistically determine cell identity in Arabidopsis. PLoS Genet **5,** e1000605.

Airoldi, C.A., McKay, M., and Davies, B. (2015). MAF2 Is Regulated by Temperature-Dependent Splicing and Represses Flowering at Low Temperatures in Parallel with FLM. PLoS One **10,** e0126516.

An, H., Roussot, C., Suarez-Lopez, P., Corbesier, L., Vincent, C., Pineiro, M., Hepworth, S., Mouradov, A., Justin, S., Turnbull, C., and Coupland, G. (2004). CONSTANS acts in the phloem to regulate a systemic signal that induces photoperiodic flowering of Arabidopsis. Development **131,** 3615-3626.

Anders, S., Pyl, P.T., and Huber, W. (2015). HTSeq--a Python framework to work with high-throughput sequencing data. Bioinformatics **31,** 166-169.

Andres, F., and Coupland, G. (2012). The genetic basis of flowering responses to seasonal cues. Nat Rev Genet **13,** 627-639.

Andres, F., Porri, A., Torti, S., Mateos, J., Romera-Branchat, M., Garcia-Martinez, J.L., Fornara, F., Gregis, V., Kater, M.M., and Coupland, G. (2014). SHORT VEGETATIVE PHASE reduces

914 gibberellin biosynthesis at the Arabidopsis shoot apex to regulate the floral transition. Proc
915 Natl Acad Sci U S A **111,** E2760-2769.
916 **Aukerman, M.J., and Sakai, H.** (2003). Regulation of flowering time and floral organ identity by a
917 MicroRNA and its APETALA2-like target genes. Plant Cell **15,** 2730-2741.
918 **Balasubramanian, S., Sureshkumar, S., Lempe, J., and Weigel, D.** (2006). Potent induction of
919 Arabidopsis thaliana flowering by elevated growth temperature. PLoS Genet **2,** e106.
920 **Barton, M.K.** (2010). Twenty years on: the inner workings of the shoot apical meristem, a
921 developmental dynamo. Dev Biol **341,** 95-113.
922 **Bouche, F., Lobet, G., Tocquin, P., and Perilleux, C.** (2016). FLOR-ID: an interactive database of
923 flowering-time gene networks in Arabidopsis thaliana. Nucleic Acids Res **44,** D1167-D1171.
924 **Bowman, J.L., and Eshed, Y.** (2000). Formation and maintenance of the shoot apical meristem.
925 Trends in Plant Science **5,** 110-115.
926 **Bradley, D., Carpenter, R., Sommer, H., Hartley, N., and Coen, E.** (1993). Complementary floral
927 homeotic phenotypes result from opposite orientations of a transposon at the plena locus of
928 Antirrhinum. Cell **72,** 85-95.
929 **Carter, B., Bishop, B., Ho, K.K., Huang, R., Jia, W., Zhang, H., Pascuzzi, P.E., Deal, R.B., and Ogas, J.**
930 (2018). The Chromatin Remodelers PKL and PIE1 Act in an Epigenetic Pathway That
931 Determines H3K27me3 Homeostasis in Arabidopsis. Plant Cell **30,** 1337-1352.
932 **Chandler, J., Wilson, A., and Dean, C.** (1996). Arabidopsis mutants showing an altered response to
933 vernalization. Plant J **10,** 637-644.
934 **Chen, K., Xi, Y., Pan, X., Li, Z., Kaestner, K., Tyler, J., Dent, S., He, X., and Li, W.** (2013). DANPOS:
935 dynamic analysis of nucleosome position and occupancy by sequencing. Genome Res **23,**
936 341-351.
937 **Clough, S.J., and Bent, A.F.** (1998). Floral dip: a simplified method for Agrobacterium-mediated
938 transformation of Arabidopsis thaliana. Plant J **16,** 735-743.
939 **Coleman-Derr, D., and Zilberman, D.** (2012). Deposition of Histone Variant H2A.Z within Gene Bodies
940 Regulates Responsive Genes. Plos Genetics **8**.
941 **Collani, S., Neumann, M., Yant, L., and Schmid, M.** (2019). FT modulates genome-wide DNA-binding
942 of the bZIP transcription factor FD. Plant Physiol.
943 **Corbesier, L., Vincent, C., Jang, S., Fornara, F., Fan, Q., Searle, I., Giakountis, A., Farrona, S., Gissot,**
944 **L., Turnbull, C., and Coupland, G.** (2007). FT protein movement contributes to long-distance
945 signaling in floral induction of Arabidopsis. Science **316,** 1030-1033.
946 **Cox, J., and Mann, M.** (2008). MaxQuant enables high peptide identification rates, individualized
947 p.p.b.-range mass accuracies and proteome-wide protein quantification. Nature
948 Biotechnology **26,** 1367-1372.
949 **Daviere, J.M., and Achard, P.** (2013). Gibberellin signaling in plants. Development **140,** 1147-1151.
950 **Deng, W., Ying, H., Helliwell, C.A., Taylor, J.M., Peacock, W.J., and Dennis, E.S.** (2011). FLOWERING
951 LOCUS C (FLC) regulates development pathways throughout the life cycle of Arabidopsis.
952 Proc Natl Acad Sci U S A **108,** 6680-6685.
953 **Earley, K.W., Haag, J.R., Pontes, O., Opper, K., Juehne, T., Song, K., and Pikaard, C.S.** (2006).
954 Gateway-compatible vectors for plant functional genomics and proteomics. Plant J **45,** 616-
955 629.
956 **Eriksson, S., Bohlenius, H., Moritz, T., and Nilsson, O.** (2006). GA4 is the active gibberellin in the
957 regulation of LEAFY transcription and Arabidopsis floral initiation. Plant Cell **18,** 2172-2181.
958 **Farrona, S., Coupland, G., and Turck, F.** (2008). The impact of chromatin regulation on the floral
959 transition. Semin Cell Dev Biol **19,** 560-573.
960 **Farrona, S., Hurtado, L., Bowman, J.L., and Reyes, J.C.** (2004). The Arabidopsis thaliana SNF2
961 homolog AtBRM controls shoot development and flowering. Development **131,** 4965-4975.
962 **Favaro, R., Pinyopich, A., Battaglia, R., Kooiker, M., Borghi, L., Ditta, G., Yanofsky, M.F., Kater,**
963 **M.M., and Colombo, L.** (2003). MADS-box protein complexes control carpel and ovule
964 development in Arabidopsis. Plant Cell **15,** 2603-2611.

965 **Fernandez, V., Takahashi, Y., Le Gourrierec, J., and Coupland, G.** (2016). Photoperiodic and
966 thermosensory pathways interact through CONSTANS to promote flowering at high
967 temperature under short days. Plant J **86,** 426-440.
968 **Ferrandiz, C., Gu, Q., Martienssen, R., and Yanofsky, M.F.** (2000). Redundant regulation of meristem
969 identity and plant architecture by FRUITFULL, APETALA1 and CAULIFLOWER. Development
970 **127,** 725-734.
971 **Fu, X., Li, C., Liang, Q., Zhou, Y., He, H., and Fan, L.M.** (2016). CHD3 chromatin-remodeling factor
972 PICKLE regulates floral transition partially via modulating LEAFY expression at the chromatin
973 level in Arabidopsis. Sci China Life Sci **59,** 516-528.
974 **Galvao, V.C., Horrer, D., Kuttner, F., and Schmid, M.** (2012). Spatial control of flowering by DELLA
975 proteins in Arabidopsis thaliana. Development **139,** 4072-4082.
976 **Galvao, V.C., Collani, S., Horrer, D., and Schmid, M.** (2015). Gibberellic acid signaling is required for
977 ambient temperature-mediated induction of flowering in Arabidopsis thaliana. Plant Journal
978 **84,** 949-962.
979 **Gandikota, M., Birkenbihl, R.P., Hohmann, S., Cardon, G.H., Saedler, H., and Huijser, P.** (2007). The
980 miRNA156/157 recognition element in the 3' UTR of the Arabidopsis SBP box gene SPL3
981 prevents early flowering by translational inhibition in seedlings. Plant J **49,** 683-693.
982 **Hartwig, B., James, G.V., Konrad, K., Schneeberger, K., and Turck, F.** (2012). Fast isogenic mapping-
983 by-sequencing of ethyl methanesulfonate-induced mutant bulks. Plant Physiol **160,** 591-600.
984 **Hu, Y., Liu, D., Zhong, X., Zhang, C., Zhang, Q., and Zhou, D.X.** (2012). CHD3 protein recognizes and
985 regulates methylated histone H3 lysines 4 and 27 over a subset of targets in the rice genome.
986 Proc Natl Acad Sci U S A **109,** 5773-5778.
987 **Hyun, Y., Richter, R., and Coupland, G.** (2017). Competence to Flower: Age-Controlled Sensitivity to
988 Environmental Cues. Plant Physiol **173,** 36-46.
989 **Hyun, Y., Richter, R., Vincent, C., Martinez-Gallegos, R., Porri, A., and Coupland, G.** (2016). Multi-
990 layered Regulation of SPL15 and Cooperation with SOC1 Integrate Endogenous Flowering
991 Pathways at the Arabidopsis Shoot Meristem. Dev Cell **37,** 254-266.
992 **Hyun, Y., Vincent, C., Tilmes, V., Bergonzi, S., Kiefer, C., Richter, R., Martinez-Gallegos, R., Severing,**
993 **E., and Coupland, G.** (2019). A regulatory circuit conferring varied flowering response to cold
994 in annual and perennial plants. Science **363,** 409-+.
995 **Jaeger, K.E., and Wigge, P.A.** (2007). FT protein acts as a long-range signal in Arabidopsis. Curr Biol
996 **17,** 1050-1054.
997 **Jang, S., Torti, S., and Coupland, G.** (2009). Genetic and spatial interactions between FT, TSF and SVP
998 during the early stages of floral induction in Arabidopsis. Plant J **60,** 614-625.
999 **Jing, Y., Zhang, D., Wang, X., Tang, W., Wang, W., Huai, J., Xu, G., Chen, D., Li, Y., and Lin, R.** (2013).
1000 Arabidopsis chromatin remodeling factor PICKLE interacts with transcription factor HY5 to
1001 regulate hypocotyl cell elongation. Plant Cell **25,** 242-256.
1002 **Jing, Y.J., Guo, Q., and Lin, R.C.** (2019a). The Chromatin-Remodeling Factor PICKLE Antagonizes
1003 Polycomb Repression of FT to Promote Flowering. Plant Physiology **181,** 656-668.
1004 **Jing, Y.J., Guo, Q., Zha, P., and Lin, R.C.** (2019b). The chromatin-remodelling factor PICKLE interacts
1005 with CONSTANS to promote flowering in Arabidopsis. Plant Cell Environ **42,** 2495-2507.
1006 **Jones, M.A., Covington, M.F., DiTacchio, L., Vollmers, C., Panda, S., and Harmer, S.L.** (2010). Jumonji
1007 domain protein JMJD5 functions in both the plant and human circadian systems. Proc Natl
1008 Acad Sci U S A **107,** 21623-21628.
1009 **Kardailsky, I., Shukla, V.K., Ahn, J.H., Dagenais, N., Christensen, S.K., Nguyen, J.T., Chory, J.,**
1010 **Harrison, M.J., and Weigel, D.** (1999). Activation tagging of the floral inducer FT. Science
1011 **286,** 1962-1965.
1012 **Kaufmann, K., Muino, J.M., Osteras, M., Farinelli, L., Krajewski, P., and Angenent, G.C.** (2010).
1013 Chromatin immunoprecipitation (ChIP) of plant transcription factors followed by sequencing
1014 (ChIP-SEQ) or hybridization to whole genome arrays (ChIP-CHIP). Nat Protoc **5,** 457-472.

1015 **Kim, D., Pertea, G., Trapnell, C., Pimentel, H., Kelley, R., and Salzberg, S.L.** (2013). TopHat2: accurate
1016 alignment of transcriptomes in the presence of insertions, deletions and gene fusions.
1017 Genome Biol **14,** R36.
1018 **Klock, H.E., and Lesley, S.A.** (2009). The Polymerase Incomplete Primer Extension (PIPE) method
1019 applied to high-throughput cloning and site-directed mutagenesis. Methods Mol Biol **498,** 91-
1020 103.
1021 **Kobayashi, Y., Kaya, H., Goto, K., Iwabuchi, M., and Araki, T.** (1999). A pair of related genes with
1022 antagonistic roles in mediating flowering signals. Science **286,** 1960-1962.
1023 **Koornneef, M., Hanhart, C.J., and van der Veen, J.H.** (1991). A genetic and physiological analysis of
1024 late flowering mutants in Arabidopsis thaliana. Mol Gen Genet **229,** 57-66.
1025 **Koornneef, M., Alonso-Blanco, C., Blankestijn-de Vries, H., Hanhart, C.J., and Peeters, A.J.** (1998).
1026 Genetic interactions among late-flowering mutants of Arabidopsis. Genetics **148,** 885-892.
1027 **Kumar, S.V., Lucyshyn, D., Jaeger, K.E., Alos, E., Alvey, E., Harberd, N.P., and Wigge, P.A.** (2012).
1028 Transcription factor PIF4 controls the thermosensory activation of flowering. Nature **484,**
1029 242-245.
1030 **Kurihara, D., Mizuta, Y., Sato, Y., and Higashiyama, T.** (2015). ClearSee: a rapid optical clearing
1031 reagent for whole-plant fluorescence imaging. Development **142,** 4168-4179.
1032 **Lamesch, P., Berardini, T.Z., Li, D., Swarbreck, D., Wilks, C., Sasidharan, R., Muller, R., Dreher, K.,**
1033 **Alexander, D.L., Garcia-Hernandez, M., Karthikeyan, A.S., Lee, C.H., Nelson, W.D., Ploetz, L.,**
1034 **Singh, S., Wensel, A., and Huala, E.** (2012). The Arabidopsis Information Resource (TAIR):
1035 improved gene annotation and new tools. Nucleic Acids Res **40,** D1202-1210.
1036 **Langmead, B., Trapnell, C., Pop, M., and Salzberg, S.L.** (2009). Ultrafast and memory-efficient
1037 alignment of short DNA sequences to the human genome. Genome Biol **10,** R25.
1038 **Lee, J.H., Yoo, S.J., Park, S.H., Hwang, I., Lee, J.S., and Ahn, J.H.** (2007). Role of SVP in the control of
1039 flowering time by ambient temperature in Arabidopsis. Genes Dev **21,** 397-402.
1040 **Lee, J.H., Ryu, H.S., Chung, K.S., Pose, D., Kim, S., Schmid, M., and Ahn, J.H.** (2013). Regulation of
1041 temperature-responsive flowering by MADS-box transcription factor repressors. Science **342,**
1042 628-632.
1043 **Li, C.L., Gu, L.F., Gao, L., Chen, C., Wei, C.Q., Qiu, Q., Chien, C.W., Wang, S.K., Jiang, L.H., Ai, L.F.,**
1044 **Chen, C.Y., Yang, S.G., Nguyen, V., Qi, Y.H., Snyder, M.P., Burlingame, A.L., Kohalmi, S.E.,**
1045 **Huang, S.Z., Cao, X.F., Wang, Z.Y., Wu, K.Q., Chen, X.M., and Cui, Y.H.** (2016). Concerted
1046 genomic targeting of H3K27 demethylase REF6 and chromatin-remodeling ATPase BRM in
1047 Arabidopsis. Nature Genetics **48,** 687-+.
1048 **Li, D., Liu, C., Shen, L., Wu, Y., Chen, H., Robertson, M., Helliwell, C.A., Ito, T., Meyerowitz, E., and**
1049 **Yu, H.** (2008). A repressor complex governs the integration of flowering signals in
1050 Arabidopsis. Dev Cell **15,** 110-120.
1051 **Li, H., Handsaker, B., Wysoker, A., Fennell, T., Ruan, J., Homer, N., Marth, G., Abecasis, G., Durbin,**
1052 **R., and Proc, G.P.D.** (2009). The Sequence Alignment/Map format and SAMtools.
1053 Bioinformatics **25,** 2078-2079.
1054 **Lu, F.L., Cui, X., Zhang, S.B., Jenuwein, T., and Cao, X.F.** (2011). Arabidopsis REF6 is a histone H3
1055 lysine 27 demethylase. Nature Genetics **43,** 715-U144.
1056 **March-Diaz, R., Garcia-Dominguez, M., Lozano-Juste, J., Leon, J., Florencio, F.J., and Reyes, J.C.**
1057 (2008). Histone H2A.Z and homologues of components of the SWR1 complex are required to
1058 control immunity in Arabidopsis. Plant Journal **53,** 475-487.
1059 **Mateos, J.L., Madrigal, P., Tsuda, K., Rawat, V., Richter, R., Romera-Branchat, M., Fornara, F.,**
1060 **Schneeberger, K., Krajewski, P., and Coupland, G.** (2015). Combinatorial activities of SHORT
1061 VEGETATIVE PHASE and FLOWERING LOCUS C define distinct modes of flowering regulation
1062 in Arabidopsis. Genome Biol **16,** 31.
1063 **Mathieu, J., Warthmann, N., Kuttner, F., and Schmid, M.** (2007). Export of FT protein from phloem
1064 companion cells is sufficient for floral induction in Arabidopsis. Curr Biol **17,** 1055-1060.

1065 **Melzer, S., Lens, F., Gennen, J., Vanneste, S., Rohde, A., and Beeckman, T.** (2008). Flowering-time
1066 genes modulate meristem determinacy and growth form in Arabidopsis thaliana. Nat Genet
1067 **40,** 1489-1492.
1068 **Michaels, S.D., and Amasino, R.M.** (1999). FLOWERING LOCUS C encodes a novel MADS domain
1069 protein that acts as a repressor of flowering. Plant Cell **11,** 949-956.
1070 **Michaels, S.D., and Amasino, R.M.** (2001). Loss of FLOWERING LOCUS C activity eliminates the late-
1071 flowering phenotype of FRIGIDA and autonomous pathway mutations but not
1072 responsiveness to vernalization. Plant Cell **13,** 935-941.
1073 **Murashige, T., and Skoog, F.** (1962). A Revised Medium for Rapid Growth and Bio Assays with
1074 Tobacco Tissue Cultures. Physiol Plantarum **15,** 473-497.
1075 **Noh, Y.S., and Amasino, R.M.** (2003). PIE1, an ISWI family gene, is required for FLC activation and
1076 floral repression in Arabidopsis. Plant Cell **15,** 1671-1682.
1077 **Ogas, J., Kaufmann, S., Henderson, J., and Somerville, C.** (1999). PICKLE is a CHD3 chromatin-
1078 remodeling factor that regulates the transition from embryonic to vegetative development in
1079 Arabidopsis. Proc Natl Acad Sci U S A **96,** 13839-13844.
1080 **Onouchi, H., Igeno, M.I., Perilleux, C., Graves, K., and Coupland, G.** (2000). Mutagenesis of plants
1081 overexpressing CONSTANS demonstrates novel interactions among Arabidopsis flowering-
1082 time genes. Plant Cell **12,** 885-900.
1083 **Park, J., Oh, D.H., Dassanayake, M., Nguyen, K.T., Ogas, J., Choi, G., and Sun, T.P.** (2017). Gibberellin
1084 Signaling Requires Chromatin Remodeler PICKLE to Promote Vegetative Growth and Phase
1085 Transitions. Plant Physiol **173,** 1463-1474.
1086 **Plackett, A.R., Powers, S.J., Fernandez-Garcia, N., Urbanova, T., Takebayashi, Y., Seo, M., Jikumaru,**
1087 **Y., Benlloch, R., Nilsson, O., Ruiz-Rivero, O., Phillips, A.L., Wilson, Z.A., Thomas, S.G., and**
1088 **Hedden, P.** (2012). Analysis of the developmental roles of the Arabidopsis gibberellin 20-
1089 oxidases demonstrates that GA20ox1, -2, and -3 are the dominant paralogs. Plant Cell **24,**
1090 941-960.
1091 **Porri, A., Torti, S., Romera-Branchat, M., and Coupland, G.** (2012). Spatially distinct regulatory roles
1092 for gibberellins in the promotion of flowering of Arabidopsis under long photoperiods.
1093 Development **139,** 2198-2209.
1094 **Pose, D., Verhage, L., Ott, F., Yant, L., Mathieu, J., Angenent, G.C., Immink, R.G., and Schmid, M.**
1095 (2013). Temperature-dependent regulation of flowering by antagonistic FLM variants. Nature
1096 **503,** 414-417.
1097 **Ramirez, F., Dundar, F., Diehl, S., Gruning, B.A., and Manke, T.** (2014). deepTools: a flexible platform
1098 for exploring deep-sequencing data. Nucleic Acids Res **42,** W187-191.
1099 **Rappsilber, J., Ishihama, Y., and Mann, M.** (2003). Stop and go extraction tips for matrix-assisted
1100 laser desorption/ionization, nanoelectrospray, and LC/MS sample pretreatment in
1101 proteomics. Anal Chem **75,** 663-670.
1102 **Ratcliffe, O.J., Bradley, D.J., and Coen, E.S.** (1999). Separation of shoot and floral identity in
1103 Arabidopsis. Development **126,** 1109-1120.
1104 **Ratcliffe, O.J., Amaya, I., Vincent, C.A., Rothstein, S., Carpenter, R., Coen, E.S., and Bradley, D.J.**
1105 (1998). A common mechanism controls the life cycle and architecture of plants.
1106 Development **125,** 1609-1615.
1107 **Richter, R., Kinoshita, A., Vincent, C., Martinez-Gallegos, R., Gao, H., van Driel, A.D., Hyun, Y.,**
1108 **Mateos, J.L., and Coupland, G.** (2019). Floral regulators FLC and SOC1 directly regulate
1109 expression of the B3-type transcription factor TARGET OF FLC AND SVP 1 at the Arabidopsis
1110 shoot apex via antagonistic chromatin modifications. PLoS Genet **15,** e1008065.
1111 **Rieu, I., Ruiz-Rivero, O., Fernandez-Garcia, N., Griffiths, J., Powers, S.J., Gong, F., Linhartova, T.,**
1112 **Eriksson, S., Nilsson, O., Thomas, S.G., Phillips, A.L., and Hedden, P.** (2008). The gibberellin
1113 biosynthetic genes AtGA20ox1 and AtGA20ox2 act, partially redundantly, to promote growth
1114 and development throughout the Arabidopsis life cycle. Plant J **53,** 488-504.
1115 **Sang, Y., Silva-Ortega, C.O., Wu, S., Yamaguchi, N., Wu, M.F., Pfluger, J., Gillmor, C.S., Gallagher,**
1116 **K.L., and Wagner, D.** (2012). Mutations in two non-canonical Arabidopsis SWI2/SNF2

1117 chromatin remodeling ATPases cause embryogenesis and stem cell maintenance defects.
1118 Plant J **72,** 1000-1014.
1119 **Schmid, M., Uhlenhaut, N.H., Godard, F., Demar, M., Bressan, R., Weigel, D., and Lohmann, J.U.**
1120 (2003). Dissection of floral induction pathways using global expression analysis. Development
1121 **130,** 6001-6012.
1122 **Schneeberger, K.** (2014). Using next-generation sequencing to isolate mutant genes from forward
1123 genetic screens. Nat Rev Genet **15,** 662-676.
1124 **Schneeberger, K., Ossowski, S., Lanz, C., Juul, T., Petersen, A.H., Nielsen, K.L., Jorgensen, J.E.,**
1125 **Weigel, D., and Andersen, S.U.** (2009). SHOREmap: simultaneous mapping and mutation
1126 identification by deep sequencing. Nat Methods **6,** 550-551.
1127 **Schwarz, S., Grande, A.V., Bujdoso, N., Saedler, H., and Huijser, P.** (2008). The microRNA regulated
1128 SBP-box genes SPL9 and SPL15 control shoot maturation in Arabidopsis. Plant Mol Biol **67,**
1129 183-195.
1130 **Searle, I., He, Y.H., Turck, F., Vincent, C., Fornara, F., Krober, S., Amasino, R.A., and Coupland, G.**
1131 (2006). The transcription factor FLC confers a flowering response to vernalization by
1132 repressing meristem competence and systemic signaling in Arabidopsis. Gene Dev **20,** 898-
1133 912.
1134 **Sheldon, C.C., Burn, J.E., Perez, P.P., Metzger, J., Edwards, J.A., Peacock, W.J., and Dennis, E.S.**
1135 (1999). The FLF MADS box gene: A repressor of flowering in Arabidopsis regulated by
1136 vernalization and methylation. Plant Cell **11,** 445-458.
1137 **Smaczniak, C., Immink, R.G.H., Muino, J.M., Blanvillain, R., Busscher, M., Busscher-Lange, J., Dinh,**
1138 **Q.D., Liu, S.J., Westphal, A.H., Boeren, S., Parcy, F., Xu, L., Carles, C.C., Angenent, G.C., and**
1139 **Kaufmann, K.** (2012). Characterization of MADS-domain transcription factor complexes in
1140 Arabidopsis flower development. P Natl Acad Sci USA **109,** 1560-1565.
1141 **Srikanth, A., and Schmid, M.** (2011). Regulation of flowering time: all roads lead to Rome. Cell Mol
1142 Life Sci **68,** 2013-2037.
1143 **Suarez-Lopez, P., Wheatley, K., Robson, F., Onouchi, H., Valverde, F., and Coupland, G.** (2001).
1144 CONSTANS mediates between the circadian clock and the control of flowering in Arabidopsis.
1145 Nature **410,** 1116-1120.
1146 **Sun, H., and Schneeberger, K.** (2015). SHOREmap v3.0: fast and accurate identification of causal
1147 mutations from forward genetic screens. Methods Mol Biol **1284,** 381-395.
1148 **Torti, S., Fornara, F., Vincent, C., Andres, F., Nordstrom, K., Gobel, U., Knoll, D., Schoof, H., and**
1149 **Coupland, G.** (2012). Analysis of the Arabidopsis shoot meristem transcriptome during floral
1150 transition identifies distinct regulatory patterns and a leucine-rich repeat protein that
1151 promotes flowering. Plant Cell **24,** 444-462.
1152 **Tyanova, S., Temu, T., and Cox, J.** (2016). The MaxQuant computational platform for mass
1153 spectrometry-based shotgun proteomics. Nat Protoc **11,** 2301-2319.
1154 **Valverde, F., Mouradov, A., Soppe, W., Ravenscroft, D., Samach, A., and Coupland, G.** (2004).
1155 Photoreceptor regulation of CONSTANS protein in photoperiodic flowering. Science **303,**
1156 1003-1006.
1157 **Van Larebeke, N., Engler, G., Holsters, M., Van den Elsacker, S., Zaenen, I., Schilperoort, R.A., and**
1158 **Schell, J.** (1974). Large plasmid in Agrobacterium tumefaciens essential for crown gall-
1159 inducing ability. Nature **252,** 169-170.
1160 **Vizcaino, J.A., Csordas, A., del-Toro, N., Dianes, J.A., Griss, J., Lavidas, I., Mayer, G., Perez-Riverol,**
1161 **Y., Reisinger, F., Ternent, T., Xu, Q.W., Wang, R., and Hermjakob, H.** (2016). 2016 update of
1162 the PRIDE database and its related tools. Nucleic Acids Res **44,** D447-456.
1163 **Wagner, D., Sablowski, R.W., and Meyerowitz, E.M.** (1999). Transcriptional activation of APETALA1
1164 by LEAFY. Science **285,** 582-584.
1165 **Wang, J.W., Czech, B., and Weigel, D.** (2009). miR156-Regulated SPL Transcription Factors Define an
1166 Endogenous Flowering Pathway in Arabidopsis thaliana. Cell **138,** 738-749.
1167 **Weigel, D., Alvarez, J., Smyth, D.R., Yanofsky, M.F., and Meyerowitz, E.M.** (1992). LEAFY controls
1168 floral meristem identity in Arabidopsis. Cell **69,** 843-859.

1169 **Whittaker, C., and Dean, C.** (2017). The FLC Locus: A Platform for Discoveries in Epigenetics and
1170 Adaptation. Annu Rev Cell Dev Bi **33,** 555-575.
1171 **Wigge, P.A., Kim, M.C., Jaeger, K.E., Busch, W., Schmid, M., Lohmann, J.U., and Weigel, D.** (2005).
1172 Integration of spatial and temporal information during floral induction in Arabidopsis.
1173 Science **309,** 1056-1059.
1174 **Wilson, R.N., Heckman, J.W., and Somerville, C.R.** (1992). Gibberellin Is Required for Flowering in
1175 Arabidopsis thaliana under Short Days. Plant Physiol **100,** 403-408.
1176 **Wu, G., and Poethig, R.S.** (2006). Temporal regulation of shoot development in Arabidopsis thaliana
1177 by miR156 and its target SPL3. Development **133,** 3539-3547.
1178 **Wu, M.F., Sang, Y., Bezhani, S., Yamaguchi, N., Han, S.K., Li, Z.T., Su, Y.H., Slewinski, T.L., and**
1179 **Wagner, D.** (2012). SWI2/SNF2 chromatin remodeling ATPases overcome polycomb
1180 repression and control floral organ identity with the LEAFY and SEPALLATA3 transcription
1181 factors. P Natl Acad Sci USA **109,** 3576-3581.
1182 **Xing, S., Salinas, M., Hohmann, S., Berndtgen, R., and Huijser, P.** (2010). miR156-targeted and
1183 nontargeted SBP-box transcription factors act in concert to secure male fertility in
1184 Arabidopsis. Plant Cell **22,** 3935-3950.
1185 **Xu, M.L., Hu, T.Q., Zhao, J.F., Park, M.Y., Earley, K.W., Wu, G., Yang, L., and Poethig, R.S.** (2016).
1186 Developmental Functions of miR156-Regulated SQUAMOSA PROMOTER BINDING PROTEIN-
1187 LIKE (SPL) Genes in Arabidopsis thaliana. Plos Genetics **12**.
1188 **Yamaguchi, A., Kobayashi, Y., Goto, K., Abe, M., and Araki, T.** (2005). TWIN SISTER OF FT (TSF) acts
1189 as a floral pathway integrator redundantly with FT. Plant Cell Physiol **46,** 1175-1189.
1190 **Yamaguchi, A., Wu, M.F., Yang, L., Wu, G., Poethig, R.S., and Wagner, D.** (2009). The microRNA-
1191 regulated SBP-Box transcription factor SPL3 is a direct upstream activator of LEAFY,
1192 FRUITFULL, and APETALA1. Dev Cell **17,** 268-278.
1193 **Yamaguchi, N., Winter, C.M., Wu, M.F., Kanno, Y., Yamaguchi, A., Seo, M., and Wagner, D.** (2014).
1194 Gibberellin Acts Positively Then Negatively to Control Onset of Flower Formation in
1195 Arabidopsis. Science **344,** 638-641.
1196 **Yamaguchi, S.** (2008). Gibberellin metabolism and its regulation. Annu Rev Plant Biol **59,** 225-251.
1197 **Yan, Y., Shen, L., Chen, Y., Bao, S., Thong, Z., and Yu, H.** (2014). A MYB-domain protein EFM
1198 mediates flowering responses to environmental cues in Arabidopsis. Dev Cell **30,** 437-448.
1199 **Yoo, S.J., Chung, K.S., Jung, S.H., Yoo, S.Y., Lee, J.S., and Ahn, J.H.** (2010). BROTHER OF FT AND TFL1
1200 (BFT) has TFL1-like activity and functions redundantly with TFL1 in inflorescence meristem
1201 development in Arabidopsis. Plant J **63,** 241-253.
1202 **Yu, S., Galvao, V.C., Zhang, Y.C., Horrer, D., Zhang, T.Q., Hao, Y.H., Feng, Y.Q., Wang, S., Schmid, M.,**
1203 **and Wang, J.W.** (2012). Gibberellin Regulates the Arabidopsis Floral Transition through
1204 miR156-Targeted SQUAMOSA PROMOTER BINDING-LIKE Transcription Factors. Plant Cell **24,**
1205 3320-3332.
1206 **Zhang, H., Bishop, B., Ringenberg, W., Muir, W.M., and Ogas, J.** (2012). The CHD3 remodeler PICKLE
1207 associates with genes enriched for trimethylation of histone H3 lysine 27. Plant Physiol **159,**
1208 418-432.
1209 **Zhang, H., Rider, S.D., Jr., Henderson, J.T., Fountain, M., Chuang, K., Kandachar, V., Simons, A.,**
1210 **Edenberg, H.J., Romero-Severson, J., Muir, W.M., and Ogas, J.** (2008). The CHD3 remodeler
1211 PICKLE promotes trimethylation of histone H3 lysine 27. J Biol Chem **283,** 22637-22648.
1212 **Zhang, Y., Schwarz, S., Saedler, H., and Huijser, P.** (2007). SPL8, a local regulator in a subset of
1213 gibberellin-mediated developmental processes in Arabidopsis. Plant Mol Biol **63,** 429-439.
1214 **Zhou, J., Wang, X., Lee, J.Y., and Lee, J.Y.** (2013). Cell-to-cell movement of two interacting AT-hook
1215 factors in Arabidopsis root vascular tissue patterning. Plant Cell **25,** 187-201.

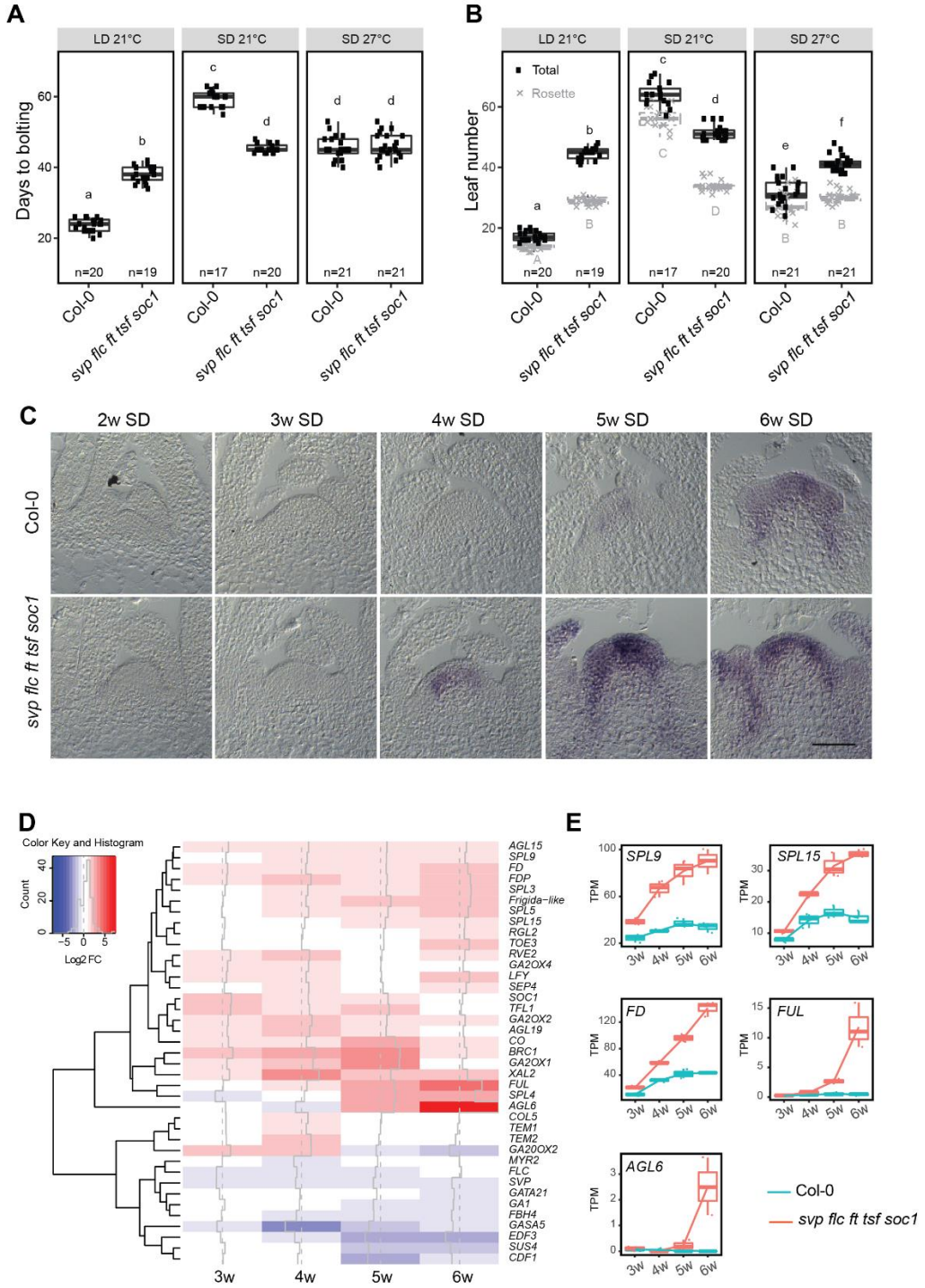

Figure 1. Phenotypic and molecular characterization of the quintuple mutant *svp flc ft tsf soc1*. **(A)** Days to bolting and **(B)** leaf number of plants grown under LD-21°C, SD-21°C and SD-27°C compared with Col-0. At least 17 plants were analyzed for each genotype. The data were analyzed with one-way ANOVA using Tukey's HSD as a post-hoc test. Different letters indicate significant differences ($p \leq 0.05$). Whiskers represent a distance of 1.5 times the interquartile range. **(C)** *In situ* hybridization analysis of *FUL* mRNA accumulation in shoot apical meristems of different genotypes grown in short days (SDs). Plants were harvested each week between 2 and 6 weeks after germination. Scale bar = 50 µm. **(D)** Transcriptional profile comparisons in apices of *svp flc ft tsf soc1.* The analysis focuses on genes implicated in flowering time control. The data are represented as a heatmap to highlight upregulated (red) and downregulated genes (blue). Gene expression changes are represented as $\log_2$-fold changes. **(E)** Box plots from RNA-seq data showing differential expression of *SPL9*, *SPL15*, *FD*, *FUL* and *AGL6* in the apices of *svp flc ft tsf soc1* and Col-0 under SDs. The Y axis shows transcripts per kilobase million (TPM). The X axis shows time of sampling as weeks after sowing. Whiskers represent distance from the lowest to the largest data point.

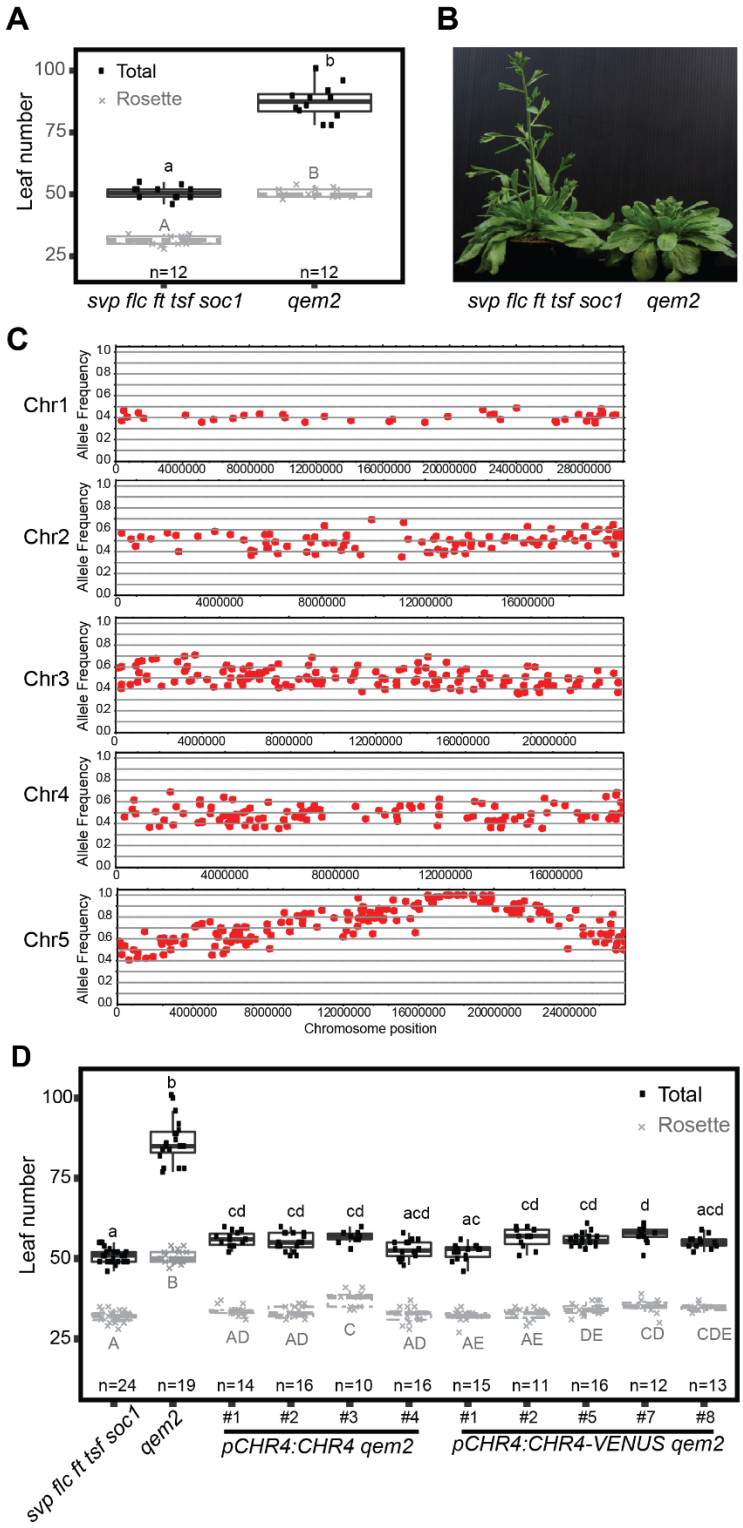

Figure 2. Molecular genetic analysis of *qem2*. (A) Leaf number at flowering of plants grown under LDs. Twelve plants were analyzed per genotype. The data were compared with one-way ANOVA using Tukey's HSD as a post-hoc test. Different letters indicate significant differences ($p \leq 0.05$). Whiskers represent the distance of 1.5 times the interquartile range. **(B)** Images of *qem2* and *svp flc ft tsf soc1* plants approximately 50 days after germination, showing that *qem2* produces more leaves than *svp flc ft tsf soc1* under LDs. **(C)** Allele frequency (AF) estimates for EMS-induced mutations. Local AFs indicate that the *qem2* mutation localized to chromosome (chr) 5. **(D)** Leaf number for *svp flc ft tsf soc1*, *qem2*, gCHR4 *qem2* and gCHR4-VENUS *qem2* plants under LDs. At least 11 plants per genotype were analyzed. The data were compared with one-way ANOVA using Tukey's HSD as a post-hoc test. Different letters indicate significant differences ($p \leq 0.05$). Whiskers represent a distance of 1.5 times the interquartile range.

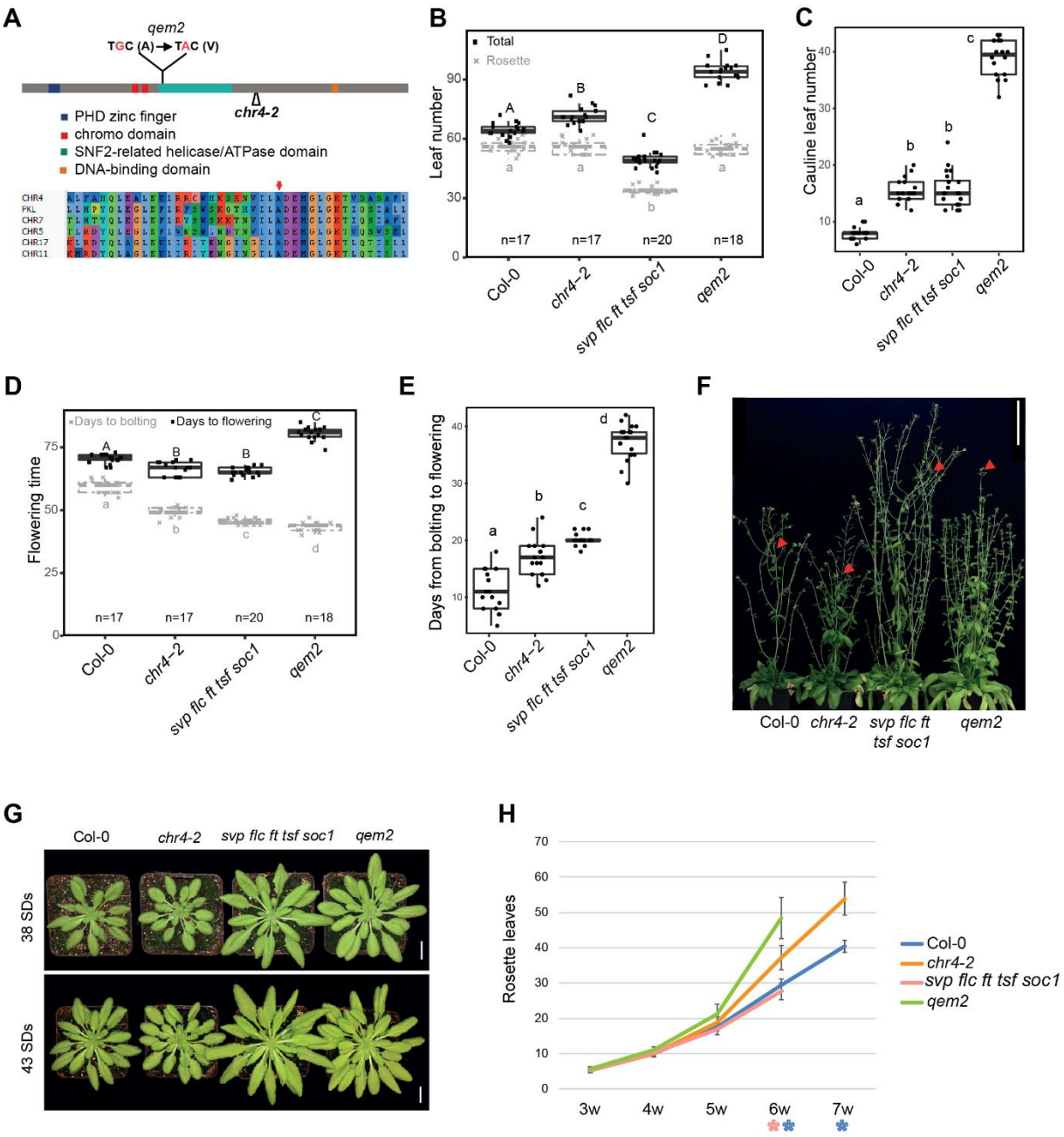

Figure 3. Characterization of CHR4. (A) Schematic representation of the *CHR4* locus showing the position of the mutation in *qem2* and the T-DNA insertion site (*chr4-2*). The CHR4 protein domains are illustrated: a plant homeodomain (PHD) zinc finger (blue), a chromo domain (red), a SNF2-related helicase/ATPase domain (green) and a DNA-binding domain (yellow). The EMS-induced protein sequence change is located within the SNF2-related helicase/ATPase domain. **(B)** Leaf number, **(C)** cauline leaf number, **(D)** days to bolting and flowering and **(E)** number of days from bolting to flowering of Col-0, *chr4-2*, *svp flc ft tsf soc1* and *qem2* plants grown under short days (SDs). At least 17 plants were analyzed for each genotype. The data were compared with one-way ANOVA using Tukey HSD as a post-hoc test. Different letters indicate significant differences ($p \leq 0.05$). Whiskers represent a distance of 1.5 times the interquartile range. **(F)** 12-week-old plants growing in SDs. Red arrows indicate first open flower. Scale bar = 10 cm **(G)** Rosettes of Col-0, *chr4-2*, *svp flc ft tsf soc1* and *qem2* plants after 38 days and 43 days of growth in SDs. Scale bar = 1 cm **(H)** Rosette leaf number of Col-0, *chr4-2*, *svp flc ft tsf soc1* and *qem2* plants grown under SDs from 3 weeks to 7 weeks. 18 plants were analyzed for each genotype. Error bars represent standard deviation of the mean. * indicates significant differences (p-value < 0.05) between Col-0 and *chr4-2* (blue) or *svp flc ft tsf soc1* and *qem2* (red).

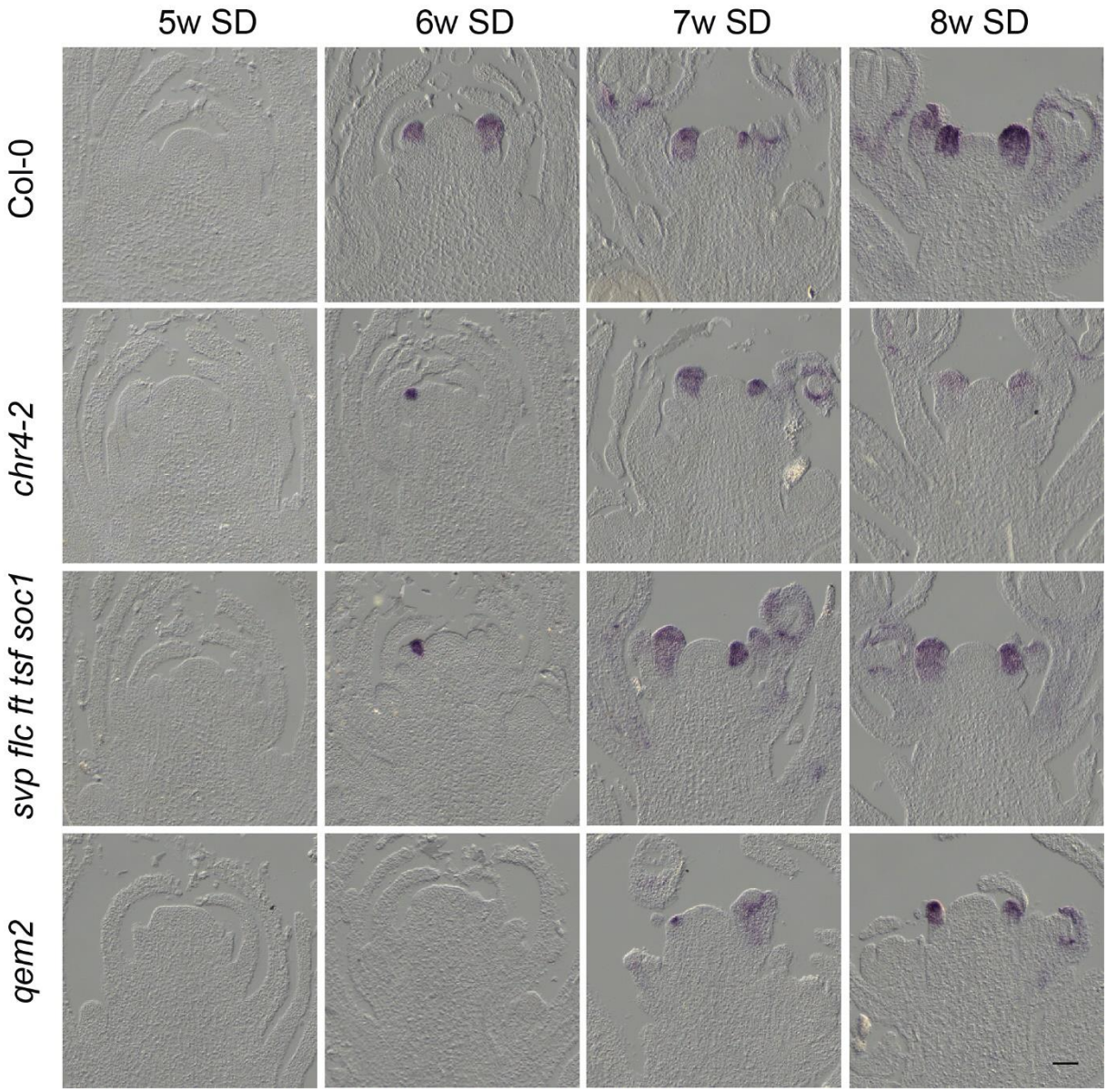

Figure 4. Temporal and spatial patterns of expression of the floral meristem identity gene *AP1* in Col-0, *chr4*-2, *svp flc ft tsf soc1* and *qem2*. *In situ* hybridization analysis of *AP1* mRNA accumulation in the shoot apical meristems of plants under SDs. The genotypes analyzed are shown together with the number of weeks (w) after germination when material was harvested. For each time point and genotype, three independent apices were examined with similar results. Scale bar = 50 µm.

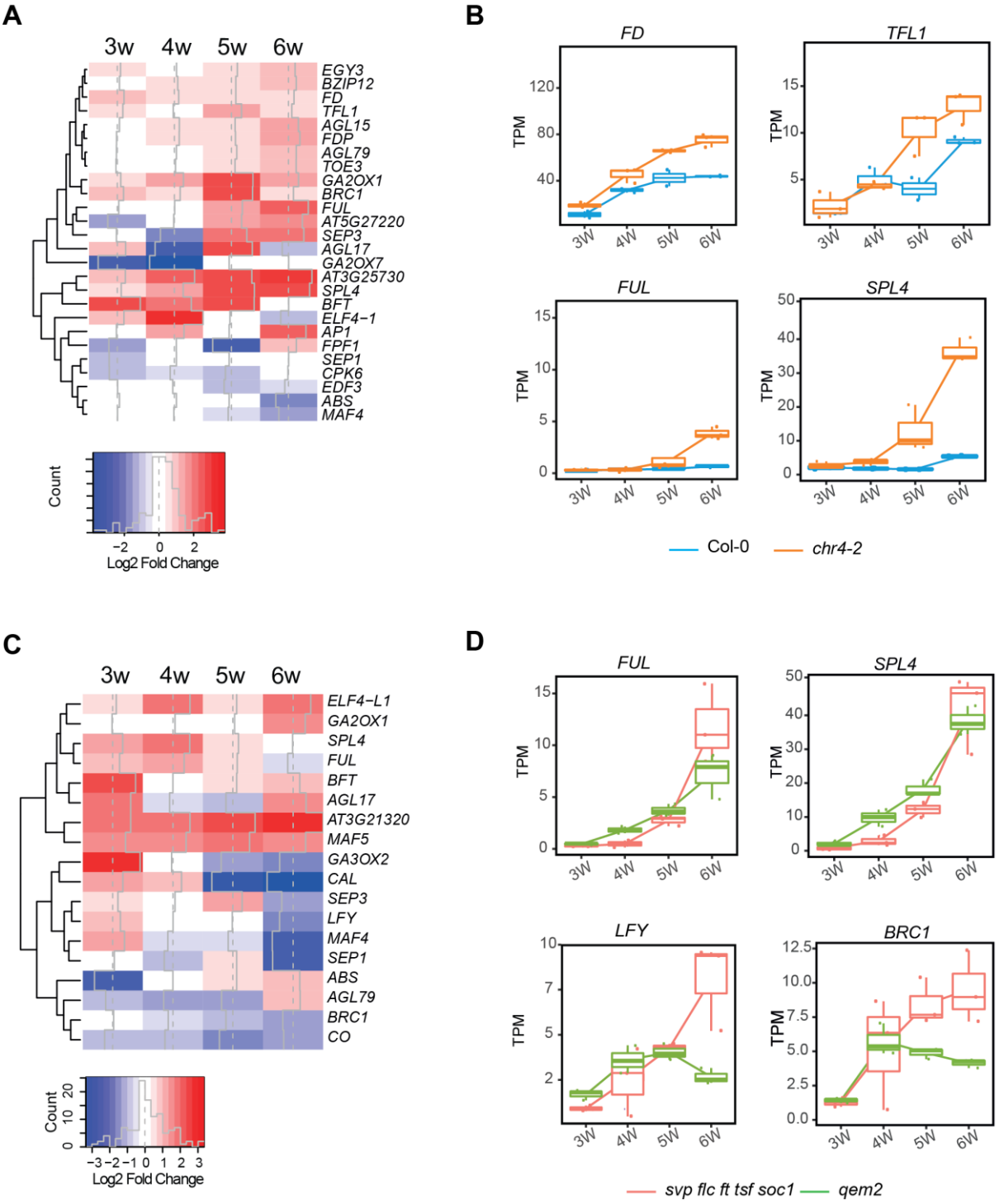

Figure 5. Transcriptional changes in *chr4* mutants. (A) Transcriptional profile comparisons represented as a heatmap to highlight genes implicated in flowering time control that are significantly upregulated (red) or downregulated (blue) in *chr4-2* compared to WT. Gene expression changes are represented as $\log_2$-fold change. **(B)** Box plots from RNA-seq data showing *FD*, *TFL1*, *FUL*, and *SPL4* transcript levels in apices of *chr4*-2 and Col-0 under SDs. The Y axis shows transcripts per kilobase million (TPM). The X axis shows time of sampling as weeks after sowing. Whiskers represent distance from the lowest to the largest data point. **(C)** Transcriptional profile comparisons represented as a heatmap to highlight genes implicated in flowering time control that are significantly upregulated (red) or downregulated (blue) in *qem2* compared to *svp flc ft tsf soc1.* **(D)** Box plots from RNA-seq data showing *FUL*, *SPL4, LFY and BRC1* transcript levels shown as transcripts per kilobase million (TPM) in apices of *qem2* and *svp flc ft tsf soc1* under SDs. The Y axis shows transcripts per kilobase million (TPM). The X axis shows time of sampling as weeks after sowing. Whiskers represent distance from the lowest to the largest data point.

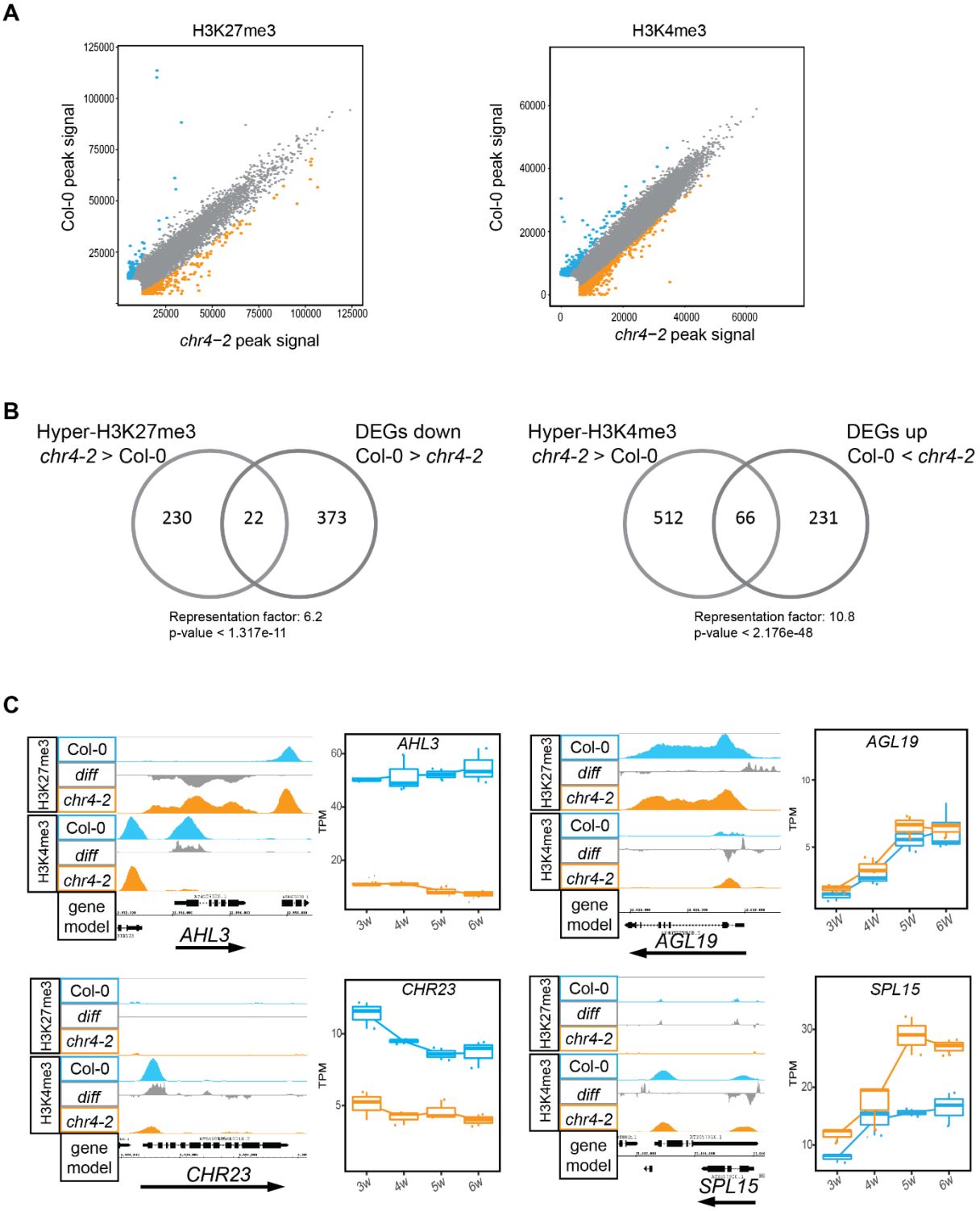

Figure 6. Histone modification variation in *chr4*-2. (A) Scatterplots showing H3K27me3 and H3K4me3 enrichment between Col-0 and *chr4-2* in apices of five- week-old plants grown under SDs. Blue and orange dots represent significantly more highly methylated regions at FDR = 0.05 in Col-0 and *chr4-2*, respectively. **(B)** Venn diagram showing the overlap between differentially expressed genes (DEGs) and genes differentially marked by H3K27me3 and H3K4me3. **(C)** H3K27me3 and H3K4me3 profiles and expression of *AHL3*, *AGL19*, *CHR23* and *SPL15*.